

RESEARCH

Open Access



Effects of long-term dehydration and quick rehydration on the camel kidney: pathological changes and modulation of the expression of solute carrier proteins and aquaporins

Hassan Abu Damir¹, Mahmoud A. Ali¹, Muna A. Adem¹, Naheed Amir¹, Osman M. Ali¹, Saeed Tariq², Ernest Adeghate², Michael P. Greenwood³, Panjiao Lin³, Fernando Alvira-Iraizoz³, Benjamin Gillard³, David Murphy^{3*} and Abdu Adem^{1,4*}

Abstract

Background Recurrent dehydration causes chronic kidney disease in humans and animal models. The dromedary camel kidney has remarkable capacity to preserve water and solute during long-term dehydration. In this study, we investigated the effects of dehydration and subsequent rehydration in the camel's kidney histology/ultrastructure and changes in aquaporin/solute carrier proteins along with gene expression.

Results In light microscopy, dehydration induced few degenerative and necrotic changes in cells of the cortical tubules with unapparent or little effect on medullary cells. The ultrastructural changes encountered in the cortex were infrequent during dehydration and included nuclear chromatin condensation, cytoplasmic vacuolization, mitochondrial swelling, endoplasmic reticulum/lysosomal degeneration and sometimes cell death. Some mRNA gene expressions involved in cell stability were upregulated by dehydration. Lesions in endothelial capillaries, glomerular membranes and podocyte tertiary processes in dehydrated camels indicated disruption of glomerular filtration barrier which were mostly corrected by rehydration. The changes in proximal tubules brush borders after dehydration, were accompanied by down regulation of ATP1A1 mRNA involved in Na⁺/K⁺ pump that were corrected by rehydration. The increased serum Na, osmolality and vasopressin were paralleled by modulation in expression level for corresponding SLC genes with net Na retention in cortex which were corrected by rehydration. Medullary collecting ducts and interstitial connective tissue were mostly unaffected during dehydration. CKD, a chronic nephropathy induced by recurrent dehydration in human and animal models and characterized by interstitial fibrosis and glomerular sclerosis, were not observed in the dehydrated/rehydrated camel kidneys. The initiating factors, endogenous fructose, AVP/AVPR2 and uric acid levels were not much affected. TGF- β 1 protein and TGF- β 1 gene expression showed no changes by dehydration in cortex/medulla to mediate fibrosis. KCNN4 gene expression level was hardly detected in the dehydrated camel's kidney; to encode for Ca⁺⁺-gated KCa3.1 channel for Ca⁺⁺ influx to instigate TGF- β 1. Modulation of AQP 1, 2, 3, 4, 9 and SLC protein and/or mRNAs expression levels during dehydration/rehydration was reported.

*Correspondence:

David Murphy
D.Murphy@bristol.ac.uk
Abdu Adem
abdu.adem@ku.ac.ae

Full list of author information is available at the end of the article



© The Author(s) 2024. **Open Access** This article is licensed under a Creative Commons Attribution-NonCommercial-NoDerivatives 4.0 International License, which permits any non-commercial use, sharing, distribution and reproduction in any medium or format, as long as you give appropriate credit to the original author(s) and the source, provide a link to the Creative Commons licence, and indicate if you modified the licensed material. You do not have permission under this licence to share adapted material derived from this article or parts of it. The images or other third party material in this article are included in the article's Creative Commons licence, unless indicated otherwise in a credit line to the material. If material is not included in the article's Creative Commons licence and your intended use is not permitted by statutory regulation or exceeds the permitted use, you will need to obtain permission directly from the copyright holder. To view a copy of this licence, visit <http://creativecommons.org/licenses/by-nc-nd/4.0/>.

Conclusions Long-term dehydration induces reversible or irreversible ultrastructural changes in kidney cortex with minor effects in medulla. Modulation of AQP channels, SLC and their mRNAs expression levels during dehydration/rehydration have a role in water conservation. Cortex and medulla respond differently to dehydration/rehydration.

Keywords Dromedary camels, Dehydration/rehydration, Kidney light microscopy and ultrastructure, Kidney aquaporins/solute carrier proteins, Gene expression

Introduction

Dehydration in animals is associated with draught in arid and semiarid areas where the grass, bushes and trees became scanty and dry and thus animals are enforced to travel for long distances searching for water and food. Dehydration is very common in camels in arid and semiarid areas but they have remarkable adaptability to this harsh dreadful environment [1–3]. In the past few years, most of livestock population died during famine in number of countries except camels [4, 5]. Again, in trading between Sudan and Egypt (durb Al Arbaein) camels used to travel for 40 days in a very tough environment with access to water only from the few scattered oases in their way.

Several hormones and peptides control the water and electrolyte reabsorption in the camel kidney, similar to other mammals, including aldosterone, vasopressin (AVP), oxytocin, Atrial Natriuretic Peptide (ANP) and B Natriuretic Peptide (BNP). The circulating levels of these hormones are altered during dehydration for the purpose of water preservation [6, 7]. Other proteins involved in water and electrolyte balance include aquaporins (AQPs) and solute carrier proteins (SLCs) encoded by many genes [8].

AQPs are water channel proteins with different sizes that facilitate water passage in the kidney. AQP1, 2 and 4 have small sized channels and selectively transport only water, whereas AQP3, 7 and 9, known as aquaglyceroporins, have wider channels to permit passage of glycerol and other small hydrophilic molecules. AQP6, 8 and 11 are located inside the cell cytoplasm with an undefined function [9]. The SLC proteins constitute over 400 members arranged in 65 families and are involved in the transmembrane transport of a diverse number of solutes including electrolytes and sugars amongst other substances [8, 10].

The camel kidney has some unique features that may enable it to cope with severe dehydration. Grossly, the camel kidney has a wider medulla relative to cortex [11], however histologically and physiologically the different units of the camel nephrons and collecting ducts are generally similar to other species. Thus, the fenestrated glomerular capillaries, the podocytes with processes and the slit diaphragm, selectively permit water, low molecular

weight proteins, electrolytes, amino acids, glucose and nitrogenous waste into bowman's space [12]. Equally, the proximal convoluted tubules with its basolateral enfolding, many mitochondria, apical brush borders and ionic pump are actively involved in reabsorption of most of the glomerular filtrate and ion transport [13]. However, the camel kidney has histological structure differences compared to other species that are thought to facilitate water/acid–base balance [12, 14]. Hence, the camel nephrons have long loops of Henle (4–6:1 camel: cattle) and vasa recta which act as counter current multiplier and counter current exchanger systems for water and electrolyte, urine concentration and oxygen passive diffusion [15, 16]. Moreover, the camel cortical tubules occupy 76% of the volume of cortex with a wider surface area (camel 9.5 vs man 8.7 m²) and a higher reabsorption capacity (88%) of glomerular filtrate by the proximal convoluted tubules [17]. In addition, the camel has higher number of glomeruli, $3.6 \pm 0.12 \times 10^6$ and wider renal corpuscles compared to other mammals (camel 220–260; man 78–168; rat $114.2 \pm 0.63 \mu\text{m}$) which enhance the renal efficiency [15, 18]. Furthermore, the juxtaglomerular apparatus in the camel, displays slight ultra-structural differences from non-desert species, with the macula densa having three types of cells (cuboidal, columnar, and pseudostratified with a single cilium) suggesting an increased efficiency of sensing Na concentration [19]. Again, the basal lamina beneath the epithelial cells of nephron is very thick compared to other species. This provides an extra support for the lumen during dehydration and rehydration, with a few anchoring sites strengthening any relatively thin areas of basal lamina in the thick loop of Henle and medullary collecting ducts [14]. Small vesicular membrane-bound bodies have also been reported in the dromedary basal lamina of the parietal cells, proximal tubules, thin loop of Henle and the juxtaglomerular apparatus, which may probably indicate their engagement in water regulation and electrolyte exchange [19, 20]. Besides that, the camel collecting ducts are 100 times more responsive to Arginine vasopressin (AVP) than collecting ducts of species such as cattle [11, 17]. The renal pelvis in the camel is enfolded to form specialized fornixes to facilitate urea cycling and urine concentration [15]. In addition, sub-mucosal serous glands of undefined role have also been

identified in the renal pelvis of the dromedary and it has been suggested to relate to water and ions regulation [21].

Dehydration can damage the mammalian kidney. Severe dehydration was reported to cause acute renal injuries, rhabdomyolysis, and hypotension with increased BUN levels in mice [22]. Similarly, acute dehydration has been reported to cause severe muscular damage with an increase in Na, BUN, LDH, CK activity in wrestlers [23]. Short-term dehydration in rabbits was reported to cause reversible flattening and spreading of podocytes and major processes with alteration of capillary permeability similar to that observed in patients with post-ischemic acute renal failure [24]. Mild dehydration with sustained high vasopressin level was suggested to induce histopathological renal lesions with albuminuria and high mortality rate in rats [25]. Moreover, recurrent dehydration, caused by heat stress has been implicated in insidious glomerular sclerosis and tubulointerstitial renal fibrosis observed in the Mesoamerican nephropathy/chronic kidney disease (CKD) [22, 26]. On the other hand, some desert rodents acquire adaptation mechanisms which help them to withstand dehydration with minimal kidney lesions if any [27, 28].

The effect of long-term dehydration and quick rehydration on kidney ultrastructural morphology has not been studied in the camel. We therefore investigated the ultrastructural changes in the kidney cortex and medulla in chronically dehydrated and rapidly rehydrated camels. In addition, we investigated whether vasopressin, kidney fructose, uric acid levels and nephrolithiasis in dehydrated/rehydrated camels contribute to the formation of kidney fibrosis/sclerosis, like that observed in humans subjected to intermittent dehydration in CKD. Finally, the possible roles of aquaporin and SLCs in water balance during long-term dehydration and quick rehydration was also investigated.

Materials and methods

Animals

Nineteen healthy male camels, 4–5 years old with body weight range of 276–416 kg, were used in this study. These camels were purchased from local owners that breed camels. These were not working camels and were not dehydrated in their life. They lived in corals where they had free access to water and alfa alfa hay. After a short adjustment period, the camels were randomly divided into three groups; Control group ($n=5$), Dehydrated group ($n=8$), and rehydrated group ($n=6$) and were assigned numbers 1C-5C for Control, 6D-13D for Dehydrated and 14R-19R for Rehydrated groups to be easily identified. The control group was supplied with dry alfa alfa and water ad libitum for the whole experimental period, the dehydrated group was also provided with dry

alfa alfa ad libitum but with complete water restriction for 20 days, whilst the rehydrated group was provided with dry alfa alfa ad libitum, completely restricted of water for 20 days and thereafter was allowed free access to water for 72 h. The animals were kept in a shaded corral during the hot months of April and May (40–50 °C) in the United Arab Emirates and maintained only on alfalfa hay during the whole experimental period and have no access to browse/graze on grass, trees or bushes. Body weights for all groups were calculated at baseline date and every five days thereafter using the formula, live weight (Kg) = Shoulder height x chest girth x hump girth $\times 50$ [29]. At the end of the experimental period, all groups were slaughtered in the Al Ain central abattoir. Camel kidney samples, as well as other tissues were obtained from all of the nineteen camels. Small pieces of the kidney were excised and then either immediately fixed in 10% (v/v) formalin, or in (2.5%) glutaraldehyde for electron microscopy, or snap-frozen in liquid nitrogen.

Health status of the animals during and after experiment

The experimental camels were closely supervised by a veterinarian from our team during the whole period of experiment. The animals age was taken from the official camel registry provided to the camel market (a read chip with all camel information). The separated areas housing the camels during the experimental period, were cleaned every morning, food provided *ad-libitum*, appetite monitored and animals observed daily for any abnormality. The animals were also checked physically when purchased and when presented for anti-mortem. We have not observed abnormal secretions and excretions from all orifices, jaundice, skin lesions, abnormal sounds, neurological signs and unusual body or urine odor. Also the vital signs, including body temperature, heart and respiratory rates were taken early morning (around 8:00 AM) at the start and end of the experimental period and were all normal. Again laboratory specimens were taken and checked before and at the end of experimental period. Blood was negative for blood parasites commonly encountered such as trypanosomiasis, flariasis, anaplasmosis and babesiosis, serological tests were negative for brucellosis, blood culture were negative for bacterial growth and feces were negative for gastrointestinal as well as skin scrapings for external parasites. It has been observed that dehydrated camels, showed reduced appetite became thinner with reduced hump, pass few hard feces, scanty concentrated urine and displayed stress behavior. Biochemical data displayed changes in number of parameters including stress hormones and antioxidants (8; 9). In the abattoir the animals passed the routine anti-mortem checks by the veterinarian in charge of the abattoir and the camels were quickly slaughtered. The

carcasses, internal organs and lymph nodes passed the routine post-mortem inspection. However, serous atrophy of perirenal and epicardial fat was observed in the dehydrated and rehydrated camels but liver lipidosis was not noticed in all animals. The meat of controls was used for human consumption while that of dehydrated and rehydrated camels were donated for Al-Ain zoo.

Chemicals, kits and antibodies

All other chemicals, if not otherwise specified, were purchased from Sigma–Aldrich Chemical Company (Sigma Chemical Co., St. Louis, MO, USA). Complete protease inhibitor cocktail was purchased from Thermo Fisher Scientific Inc. (MA, USA, 02451). Assay and ELISA kits were purchased from My BioSource, Inc. (CA, USA; Table 1).

Blood collection

Blood samples were collected via jugular venipuncture without apparent discomfort to the camels between 8:00 and 9:00 am into plain or heparinized vacutainers on ice for subsequent analysis for plasma and serum fractions. The blood in plain vacutainers was allowed to clot and serum was separated by centrifugation at 3000 rpm. The collected serum was aliquoted into clean tubes kept at -20 °C pending analyses. Blood samples collected into heparinized vacutainers were centrifuged at +4 °C shortly after collection. The plasma was decanted into clean tubes and stored at -80 °C until analyzed. Blood from control, dehydrated and rehydrated groups was collected on days 0, 5, 10, 15 and 20, and on hours 2, 12, 24, 48 and 72 after rehydration. All specimens were included in testing and statistical analyses.

Preparation of tissue homogenate

The kidney homogenate was prepared as described previously [30]. Briefly, renal tissues were washed with phosphate buffer saline (PBS), the cortex and medulla were dissected. The tissue was weighed and homogenized in an extraction buffer containing complete protease inhibitor cocktail. The homogenates obtained were centrifuged

and the supernatant stored at -80°C until further experiments.

Preparation of grids for Transmission Electron Microscope

Kidney tissue of camel were dissected out and washed with 0.1M phosphate buffer at pH 7.2 and then immersed immediately in the Carnovsky's fixative at pH=7.2 [31, 32] for 24 h at 4°C in the refrigerator. After rinsing with phosphate buffer, the tissues were post fixed with 1% (w/v) osmium tetroxide for 1 h. After washing with distilled water, the tissues were dehydrated in a series of graded ethanol from 30% (v/v) to 95% (v/v) and 100% (v/v). They were later treated with propylene oxide. The tissues were then infiltrated and embedded in Agar 100 epoxy resin and polymerized at 65°C for 24 h. Blocks were trimmed and semi thin & ultrathin sections were cut with Reichert Ultra- cuts, ultra-microtome. Semi-thin Sects. (130 nm thickness) on glass slides were stained with 1% (v/v) aqueous toluidine blue on an electrothermal slide drying bench at 55°C and ultrathin sections of golden color (95nm thin) on 200mesh Cu grids then were contrasted with uranyl acetate [33], [34] and followed by lead citrate [35] double stain. The grids were then studied/examined and photographed at different magnification under the Philips CM10 Transmission Electron Microscope (Netherlands).

Biochemical analysis of serum and plasma

Biochemical analyses of serum glucose (Glu), Blood urea nitrogen (BUN), Creatinine (Cr), Sodium (Na), Potassium (K), and Chloride (Cl) were performed using a fully automatic chemistry analyzer (Roche – Lab Cobas-C501- USA). Osmolality in serum was calculated as per the following equation: $2Na + BUN + \text{glucose}$ (all parameter in mmol/L).

Measurement of plasma Arginine vasopressin (AVP)

The levels of plasma AVP were quantified by a My BioSource Camel ELISA kits (MBS9350140) according to the manufacturer instructions. Briefly, samples and standards were added to the coated 96 well micro titer plate for 1 h. at 37 °C. After washing, removal of samples,

Table 1 MyBioSource assay and ELISA kits were used in this study

Description	Catalog#
General Fructose Assay Kit 100 Assays	MBS8243183
General Uric Acid Assay Kit 100 Assays	MBS8243236
Camel Solute Carrier Family 26 Member 6 (SLC26A6) ELISA Kit 96-Strip-Wells	MBS9367953
MyBioSource, Camel Neutrophil Gelatinase Associated Lipocalin (NGAL) ELISA Kit; 96-Strip-Wells	MBS104113
Camel High Sensitivity C-Reactive Protein (CRP) ELISA Kit 96-Strip-Wells	MBS097957
Camel Kidney Injury Molecule 1 (KIM 1) ELISA Kit; 96-Strip-Wells	MBS059436

detection reagent A, followed by reagent B were added for 15 min at 37 °C. The absorbance was read at 450 nm, after adding stop solution, with an Emax Plus microplate reader (Molecular devices, CA 94089 USA). Results were expressed as pg/ml plasma.

Measurement of plasma uric acid

A MyBioSource assay kit (MBS8243236) was used to measure plasma Uric acid according to the manufacturer's protocol. The assay reaction was initiated with the enzymatic catalysis of uric acid by uricase. The enzyme catalyzed reaction products quinone was measured at 505 nm by using a Tecan Infinite M200 Pro microplate reader (Tecan Group Ltd., Männedorf, Switzerland). The levels of plasma Uric acid were expressed as (mmol/L).

Measurement of fructose in kidney cortex and medulla homogenates

The assay for fructose was performed by using fructose assay kit (MBS8243183) according to the manufacturer's protocol with minor modification. Kidney, cortex and medulla, tissue was washed with ice-cold phosphate buffer saline (PBS) and cortex and medulla were separated. The tissue was weighed and homogenized with 10 volumes of ice-cold high KCl lysis buffer (10 mM Tris-HCl, pH 8.0, 140 mM NaCl, 300 mM KCl, 1 mM EDTA, 0.5% v/v Triton X-100 and 0.5% w/v sodium deoxycholate) with complete protease inhibitor cocktail with a polytron homogenizer (IKA laboratory, Germany). The resulting homogenates, after 30 min incubation on ice, were centrifuged at 15,000 rpm for 30 min at 4 °C. The resulting supernatant was incubated in water bath at 80 °C for 10 min, centrifuged at 4000 g for 10 min at room temperature, then used for Fructose assay according to the kit instruction. The absorbance was read at 492 with an Emax Plus microplate reader (Molecular devices, CA 94089, USA). Results were expressed as µg per milligram of tissue.

Measurement of aquaporins, solute carrier proteins and arginine vasopressin receptor 2 (AVPR2) in kidney cortex and medulla homogenates

AQP1 (MBS095603), AQP2 (MBS085081), AQP3 (MBS084810), AQP4 (MBS084444), AQP7 (MBS9362113), AQP9 (MBS068548), SLC9A9 (MBS9350780), SLC26A6 (MBS9367953) and AVPR2 (MBS9363909) measurements were performed by using precoated quantitative sandwich ELISA kits according to manufacturer's protocol (MyBioSource, Inc., CA, USA). The absorbance was read with an Emax Plus microplate reader (Molecular devices, CA 94089, USA). Results were expressed as pico- or nanogram per milligram of tissue.

Measurement of CRP in Kidney cortex and medulla homogenates

A MyBioSource Camel ELISA kit (MBS097957) was used to measure the levels of CRP in kidney homogenates and plasma in accordance with the manufacturer's protocol. Briefly, samples and standards were added to the coated 96 well micro titer plate for 1 h. at 37 °C. After washing, removal of samples, detection reagent A followed by reagent B were added for 15 min at 37°C. The absorbance was read at 450 nm, after adding stop solution, with an Emax Plus microplate reader (Molecular devices, CA 94089 USA). The levels were expressed as □g/mg of tissue or pg/ml plasma.

Measurement of Biomarkers of kidney injury in cortex and medulla homogenates

Enzyme immunoassay of kidney injury molecule-1 (KIM-1) (MBS059436) and neutrophil gelatinase-associated lipocalin (NGAL) (MBS104113) in samples were performed by using MyBioSource camel sandwich ELISA kits according to the manufacturer's protocol. Results were expressed as pg or ng per milligram of tissue.

Measurement of TGFβ and SGLT2 in kidney homogenate

ELISAs for TGFβ (MBS087558) and SGLT2 (MBS059315) was performed in the kidney cortex and medulla homogenate samples. Briefly, the assay was carried out by adding 50 µl of either standard or sample to the coated 96 well micro titer plate. HRP-conjugate reagent (100 µl) was added to every well except blank wells and incubated for 60 min at 37 °C. After washing, removal of samples, 50 µl chromogen solution A and chromogen solution B were added to each well. The plate was incubated for approximately 15 min at 37 °C. The absorbance was read at 450 nm, after adding stop solution, with an Emax Plus microplate reader (Molecular devices, CA 94089 USA). Results were expressed as ng/mg protein.

RNA extraction and cDNA synthesis

RNA extraction and cDNA synthesis were performed as described earlier [30]. Briefly, total RNA was extracted by using a Direct-zol™ RNA MiniPrep kit (Zymo research; R2052) following the manufacturer's instructions. For cDNA synthesis, 1000 ng of RNA from each sample was reversely transcribed using the GOScript™ cDNA synthesis system (Promega; A276A).

Quantitative reverse transcription PCR (qRT-PCR) analysis

Primers (Tables 2 and 3) were designed based on National Center for Biotechnology Information (NCBI)

Table 2 Primers for qPCR: for genes with multiple transcript variants, primers were designed based on the common sequences shared between all transcript variants

Gene symbol	Gene name	Reference sequence accession ID (NCBI, Ensembl)	5' to 3' primer sequence (F: forward, R: reverse)	Product size (bp)
<i>PPIA</i>	Peptidylprolyl isomerase A	XM_010987886.1	F: ACCACCAGACCATTCTTCT R: TATGGAACCCCGAAAACCTGC	109
<i>CLDN4</i>	Claudin 4	XM_010980769.2	F: CATCTGCATCATCTTGGCCG R: CTCTCATCCTCCACGCAGTT	81
<i>CILP2</i>	Cartilage intermediate layer protein 2	XM_010997357.2	F: GAAGGTTTCATCATTGCGCCC R: TGAACCAGGATGTCCACTCG	82
<i>MRPL57</i>	Mitochondrial ribosomal protein L57	XM_031465729.1	F: CAGGCGAAGCGAAACATGG R: CTGCTCGGCTGTGAGGTAG	87
<i>NRTN</i>	Neurturin	XM_031437035.1	F: GTCTACGACCTGGGCCTG R: CACCTCGTCTCGTAGGC	105
<i>SDHA</i>	Succinate dehydrogenase complex flavoprotein subunit A	XM_031442368.1 XM_031442370.1	F: GGATTTCAAGGAGCGGGTTG R: TCAACGTAGAAAGCGTGTG	108
<i>SLC2A11</i>	Solute carrier family 2 member 11	XM_031442332.1	F: TACATGGTTTGCAGGTGCT R: CACGTAGAGGAAGTGGGACA	96
<i>AMPD2</i>	Adenosine monophosphate deaminase 2	XM_031457751.1 XM_031457752.1 XM_031457753.1 XM_031457754.1 XM_010975916.2 XM_010975917.2 XM_031457755.1	F: AGTCTAAGCCCGAGAACCAC R: AGTAGGCATAGGGTGGGTTG	87
<i>NTSDC2</i>	5'-nucleotidase domain containing 2	XM_010985270.2	F: GCCAACTCTTTGACGTGGTC R: GCAGTACGCCCTTCTCATCA	99
<i>SLC17A3</i>	Solute carrier family 17-member 3	XM_010980146.2 XM_010980147.2 XM_031435092.1 XR_004131242.1 XM_031435093.1	F: GAACTCTCCCTCTTCAGCA R: CGGACTGACATAGTGGGCTT	114
<i>ATP1A1</i>	ATPase Na ⁺ /K ⁺ transporting subunit alpha 1	XM_010980699.2	F: GCATGGCGACAAAAAGAAGG R: AAGTCTGTCCCGTATTGCG	120
<i>SLC6A6</i>	Solute carrier family 6-member 6	XM_031470987.1 XM_031470988.1 XM_031470989.1 XM_031470990.1 XM_031470992.1	F: GAACTGGGTGCTCTGAAGTG R: GCGGTGAAGTAGACGACCTT	116
<i>SLC8A1</i>	Solute carrier family 8 member A1	XM_031466892.1 XM_031466893.1 XM_031466894.1 XM_031466895.1 XM_031466896.1 XM_031466897.1 XM_031466898.1 XM_031466899.1 XM_031466900.1 XM_031466901.1 XM_031466902.1 XM_031466903.1 XM_031466904.1 XM_031466905.1 XM_031466906.1 XM_031466907.1 XM_031466908.1 XM_031466909.1 XM_031466910.1	F: TCATCATCGCGCTTTGTGT R: TGCAAAGATGCTCCAAGCTG	101
<i>SLC20A1</i>	Solute carrier family 20-member 1	XM_031441258.1 XM_031441259.1	F: GACAGAAAAGGCAGTGGCAG R: TGCAGGAACTGGAAGAGGAG	83

Table 2 (continued)

Gene symbol	Gene name	Reference sequence accession ID (NCBI, Ensembl)	5' to 3' primer sequence (F: forward, R: reverse)	Product size (bp)
KCNIP4	Potassium voltage-gated channel interacting protein 4	XM_010991040.2 XM_031436695.1 XM_010991042.2 XM_031436708.1 XM_010991043.2 XM_010991044.2	F: GATACGGACCACAATGGAGC R: TACTGTCCCCCGAAGCAAAA	75
AVPR2	Arginine vasopressin receptor 2	XM_010991454.2	F: CCTGCCCAACTCTTCATCT R: CAATCCAGGTGACGTAGGCA	116
SLC26A6	Solute Carrier Family 26 Member 6	ENSCDRT00005022863.1 ENSCDRT00005023033.1	F: AGATGCCCCACTACTCTGTC R: ACCTCCCTGGCTTCTGAGTA	85
PCDH8	Protocadherin 8	ENSCDRT00005018746.1	F: CCTTTTCCCTTGCAGCTTT R: GAAGGTGCTGTATCGCACTG	79
ANGPTL4	Angiopoietin Like 4	XM_010978268.2	F: TGCCCTTCTCTACTTGGGAC R: TACTGGCCGTTAAGGTTGGA	118
AQP5	Aquaporin 5	XM_010989703.1	F: AGCGTCTACAAATCTCCGT R: GTGATGGCAGGTTGATGTG	98
AQP6	Aquaporin 6	XM_010989702.1	F: TCTGTGGCATCCCTAAAA R: CCAGATGAGACTCCAGTGGT	121
AQP7	Aquaporin 7	XM_010975828.1 XM_010975829.1 XM_010975830.1	F: CCCATCTCTGTATCGCCTGA R: GGGGACGGGATCACAGATA	110
AQP11	Aquaporin 11	XM_010990022.1	F: CTGGGGCTGACCAAGTATCA R: GGCCTCTATGACTACCGCTT	93

Table 3 The levels of BUN, Cr, Na, K, Cl, glucose and calculated osmolality of control, dehydrated and rehydrated Camels (M±SEM). Significant difference from control is denoted by **p* < 0.05, ***p* < 0.01, ****p* < 0.001 and from Dehydrated (Day 20) group by †*p* < 0.05, ††*p* < 0.01, †††*p* < 0.001

Test	Control	20 D (Dehyd)	2 h (Rehyd)	12 h (Rehyd)	24 h Rehyd	48 h (Rehyd)	72 (hrs Rehyd)
BUN mg/dl	28.6±0.7	45.1±2.9***	47.5±5.1*	39.7±5.7	37.0±3.4	28.6±3.2††	24.8±2.5†††
Cr mg/dl	1.3±0.1	3.0±0.2***	3.4±0.2***	3.6±0.2***	3.0±0.1***	2.6±0.1***	2.1±0.1***†††
Na mmol/l	154.7±0.44	173.1±0.7**	170.3±2.3**	154.2±3.8	149.2±1.8†	142.6±1.7†	145.5±1.7†
K mmol/l	4.4±0.1	4.3±0.1	4.1±0.1	7.0±0.8*	5.1±0.2**	4.8±0.2*	4.51±0.3
Cl mmol/l	114.8±0.4	130.5±0.9**	129.4±2.1**	112.9±4.2	110.3±1.9†	106.82±2.0†	108.3±2.1
Gluc g/dl	100.4±3.3	87.2±5.6*	138.8±15.2††	91.6±22.2	103.0±11.3	115.0±13.7†	121.6±16.6†
Osmolality mmol/l	327.7±1.1	371.2±6.1***	365.2±5.7***	326.0±7.9††	317.3±4.3†††	301.8±4.3†††	306.6±3.9†††
AVP (pg/ml)	25.2±0.5	27.8±0.8**	30.4±1.0***	25.9±0.6	28.2±0.9*	28.6±0.8*	29.4±0.9***

reference sequences (RefSeq) and the genome assembly Camdro2 (GCA_000803125.2) for target genes and were synthesized by Sigma-Aldrich®. The optimization and validation of primers performed according to normal ABI protocols and the relative standard curve method [36, 37]. For cDNA synthesis, 1000 ng of RNA from each sample was reversely transcribed using the GOScript™ cDNA synthesis system (Promega; A276A). The cDNA samples from reverse transcription were used as templates for the RT-qPCR which was conducted in duplicates in 12 µl reaction volumes using PowerUp™ SYBR Green Master Mix (Thermo

Fisher Scientific; 100,029,283) on an ABI StepOne-Plus Real-Time PCR System. The housekeeping gene PPIA was used as the internal control gene for RT-qPCR [38]. 2-ΔΔCT method applied for the relative quantification of gene expression [39, 40].

Statistical analysis

All statistical analyses were performed by independent *t*-test using SPSS (Statistical Package for Social Sciences, version 23: SPSS, Chicago, USA) software. Statistical analysis for RT-qPCR was performed by two-way, unpaired *t*-test with Welch correction using

Graphpad Prism 8 software. Data are expressed as mean ± SEM, and *P* value less than 0.05 was considered statistically significant.

Results

The initial body weight (kg) of treatment groups were not significantly different at day 0 (356.8 ± 4.59 control vs 363.6 ± 3.57 dehydrated groups). The dehydrated camels showed average body weight loss of 112.6 kg at day 20 versus their initial weights at day 0 (251.8 ± 8.87 vs 363.6 ± 3.57; *P* < 0.001) and a significant body weight loss compared to that of controls at days 0 (251.8 ± 8.87 vs 356.8 ± 4.59; *P* < 0.001) and at day 20 of experiment (251.8 ± 8.87 vs 364.8 ± 3.14; *P* < 0.001).

Light and electron microscopy

Images of the glomerular epithelium of control, dehydrated and rehydrated camels stained with toluidine blue, and H&E are presented in (Fig. 1) In control group (1a, 1g), the glomeruli, proximal convoluted and distal convoluted tubules exhibited normal texture, whilst in the dehydrated camels (1b, 1h) fatty degeneration and focal necrosis were evident in some glomeruli, proximal and distal convoluted tubules showed some casts in lumen. However, these lesions improved with rehydration (1c, 1i). No interstitial fibrosis or glomerular sclerosis were observed.

Glomeruli: transmission electron micrograph

Electron microscopy revealed normal and intact glomeruli ultrastructure, well-defined glomerular membrane between capillary endothelial and visceral epithelial

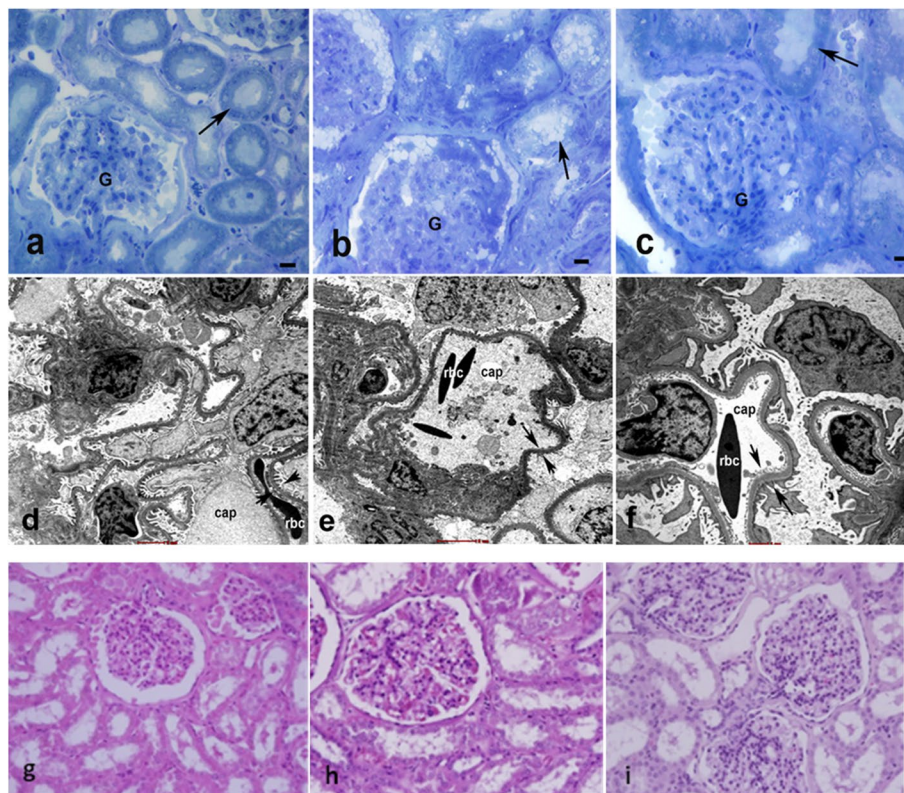


Fig. 1 **a, b, c** shows light micrographs of the cortex of the camel kidney. In the control camel group **1(a)**, the glomeruli, proximal convoluted and distal convoluted tubules (arrow) exhibited normal texture, whilst in the dehydrated camels **1(b)**: Vacuolar degeneration is discernible in the epithelium of proximal convoluted tubules (arrow) showed some casts in lumen. In the rehydrated camels **1(c)**: The epithelium of the proximal convoluted tubules (arrow) appears normal when compared to **1(a)** and **1(b)**. No interstitial fibrosis or glomerular sclerosis was observed. G = glomeruli, arrow = convoluted tubules; bar = 100 μm (**a-c**). **d, e, f** electron microscopic micrographs of the cortex of the camel kidney: **d**: shows glomerulus with an intact filtration barrier (space between 2 arrows) of normal, untreated camel; **e** glomeruli have a disrupted filtration barrier (space between 2 arrows) of dehydrated camel; **f** glomeruli have intact filtration barrier (space between 2 arrows) of rehydrated camel. Filtration barrier = endothelial cell lining + glomerular basement membrane + tertiary podocyte processes. Scale bar = 1 μm (**d-f**). **g, h, i** H&E-stained sections (x400) of control, dehydrated and rehydrated camel kidney. (**g**) No lesions were observed. Fatty degeneration, focal necrosis in some glomeruli and casts in tubular lumen in the dehydrated (**h**) group. No pathological changes were evident in glomeruli, proximal and distal tubules of rehydrated camels (**i**). No fibrosis or sclerosis were evident in the kidney of control, dehydrated or rehydrated groups.

cells, and podocytes (Fig. 1d). Capillary loops were finely fenestrated and exhibited a uniformly organized endothelial layer with a prominent nucleus and evenly distributed chromatin material. The podocytes, with a pale large nucleus on the visceral layer, possessed a normal and prominent primary and secondary foot processes arranged along the glomerular basement membrane and connected with the glomerular membrane by a thin filtration slit diaphragm. The slightly dark mesangial cells, containing amorphous mesangial matrix, were centrally located among the capillary loops and had direct contact with the endothelial cells.

In the dehydrated group (Fig. 1e), the micrographs of glomeruli revealed a large lumen of capillary loop sometimes with thin RBCs. Mostly, the endothelial fenestrations looked damaged or deteriorated and the nuclear chromatin of the capillary endothelial cell was either condensed, degenerated, or damaged. In some areas, the glomerular basement membrane looked thickened, irregular, and vacuolated. Some podocytes exhibited degenerated mitochondria, lysosomes, rough endoplasmic reticulum, and cytoplasmic vacuolization with smaller size pyknotic nuclei and with peripherally condensed chromatin. The presence of podocytic foot processes were mostly evident, however, in some cases they were fewer in number, detached, damaged or lacking. The nuclei of some mesangial cells seemed to be pyknotic, vacuolated, fragmented and indented in appearance. The overall changes in capillaries, glomerular membranes and podocyte tertiary processes may indicate disruptor of filtration barrier of some glomeruli.

In the rehydrated camel (Fig. 1f) groups, most of the capillary loops were seen normal but slightly widened at some regions in some cases. The endothelial cell nuclei looked normal and intact but rarely showed indentation and/or with condensed chromatin. Generally, the fenestrations looked normal but rarely seemed to be fewer in number, lost or disorganized. Luminal RBCs looked normal but occasionally they were swollen or marginally invaginated. Podocytes looked normal with well-defined nuclei and abundant cytoplasm. However, in some podocytic cells, the nuclei were indented or showing unevenly distributed chromatin material and/or with cytoplasmic vacuolization. The endoplasmic reticulum (ER) and mitochondria were generally normal, but some looked swollen. The foot processes were also normal and uniformly distributed over the glomerular basement membrane however, in rare cases the pedicles were detached, disorganized, and rarely degenerated. Most of the mesangial cells looked normal but some contained vacuoles and indented or variable size nuclei. Generally, the glomerular membrane was normal, however sometimes it appeared thickened, swollen or variable in size. The overall picture

may indicate that the filtration barrier resumed near normal physiological function by rehydration.

Proximal tubules: transmission electron micrograph

In controls (Fig. 2a), the transmission electron micrographs showed normal proximal convoluted tubules with well-defined long cuboidal epithelial cells bearing intact nucleus depicting well-distributed chromatin material, thick basement membrane and apical densely packed striated brush borders extending towards the tubular lumen. Numerous well-developed, intact membrane bound mitochondria with prominent cristae were located between the enfolding of basolateral plasma membranes of adjacent cells with fine tight junctions. Abundant lysosomal bodies, endosomes, rough endoplasmic reticulum, ribosomes, and peroxisomes were exhibited throughout the cytoplasm. Prominent cytoplasmic vesicles were discernable in the basal compartment within the enfolding of the basement membrane. Synaptic complexes were abundant at the apical surface of the cells near the brush border and extensive lateral interdigitating membranes were observed between neighboring cells without the appearance of distinct cell margins.

The transmission electron micrographs of the proximal tubules of dehydrated camels (Fig. 2b) displayed some abnormal cuboidal cells with thin degenerated or broken and detached brush borders extending from the surface of the apical plasma membrane towards the lumen. The nuclei of some of these cells showed condensed chromatin, pyknosis, karyorrhexis, karyolysis and/or ruptured nuclear membrane and membrane bound bodies. Fewer swollen mitochondria with broken/ degenerated cristae, were vacuolated or fused together to form enormous cytoplasmic vacuoles. The ER was unevenly distributed, fragmented or absent and fewer degenerated lysosome with irregular membranous outline were evident. Close to the apical plasma membrane, the interdigitating membranes and synaptic complexes of adjacent cells were visualized abundantly in some but rarely evident in other micrographs. The basement membrane permeated with collagenous fibers displayed variable sizes; being very short, thin and broken at some area with wavy shapes. Cytoplasmic debris with fragmented cytoplasmic organelles were pushed out into the tubular lumen.

Electron micrographs of rehydrated camel proximal tubules (Fig. 2c) depicted normal nuclei with evenly distributed chromatin material. However, in few cases the nuclear chromatin was irregularly condensed, the nuclei were small, pyknotic, indented or showed karyorrhexis. In some tubules, the lumen was filled with dead matrix. Most apical membranes displayed

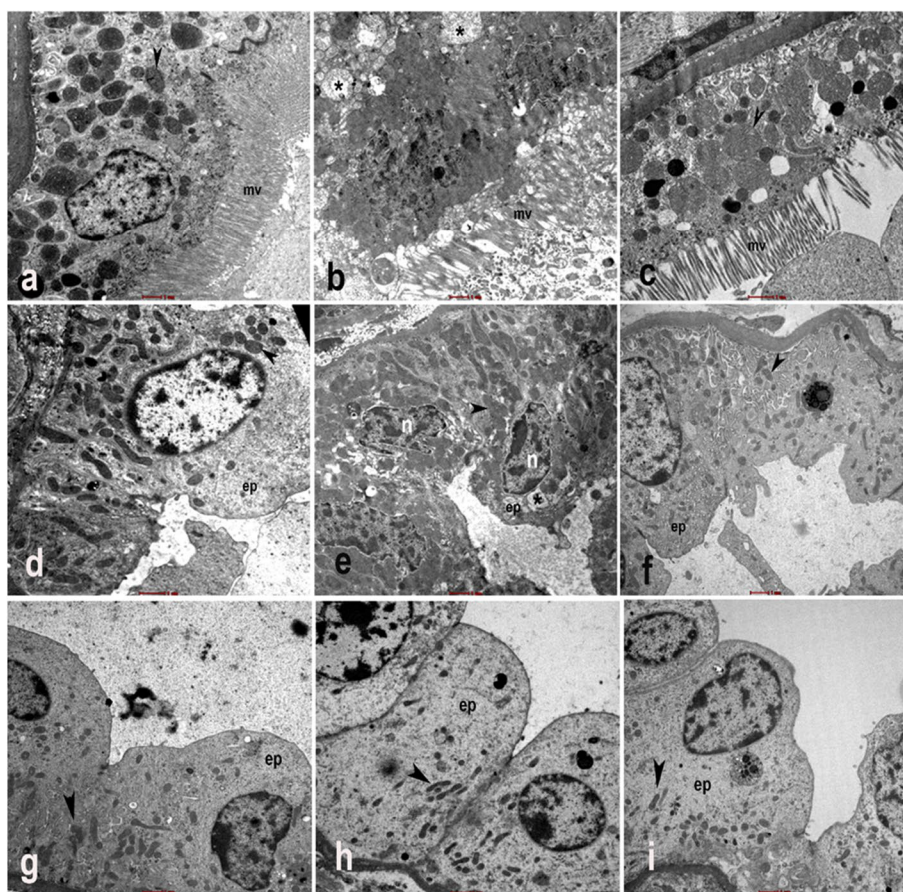


Fig. 2 shows electron micrographs of the proximal convoluted tubules (PCT, **a-c**), distal convoluted tubules (DCT, **d-f**) and collecting ducts (CD, **g-i**) of the camel kidney; **a** PCT of normal, untreated camel with intact mitochondria (arrowhead) and microvilli (mv); **b** PCT of dehydrated camels with degenerated mitochondria (arrowhead) and microvilli (mv) dotted with vacuoles; **c** PCT of rehydrated camels have near normal mitochondria (arrowhead) and microvilli (mv); **d** DCT of normal, untreated camels with intact cytoplasmic organelles; **e** DCT of dehydrated camels with bigger mitochondria (arrowhead) and pyknotic nuclei (n); **f** DCT of rehydrated camels with almost intact cytoplasmic organelles. The CD in normal (**g**), dehydrated (**h**) and rehydrated (**i**) camels appear to be intact. ep = epithelium; cap = capillary, n = nucleus. Scale bar = 1 μm

abundant brush borders with normal appearance and showing vesicles, however, in few apical plasma membrane regions, the brush borders looked partially damaged or lacking along with lack of vesicles. Many mitochondria were normal in shape; however, few of them were small, vacuolated and partially or completely degenerated. ER appeared normal and well distributed throughout the cytoplasm. Most of the lysosomes looked normal and well distributed in cell cytoplasm but in very rare occasions, they displayed abnormal shapes. Vacuoles were abundantly observed in the cytoplasm. Most of the basement membranes were normal in structure but sometimes they were wavy and invaginated. Well-defined synaptic complexes and normal interdigitating membranes between cells could be visualized except in few areas where they were deteriorated.

Distal tubules: transmission electron micrograph

The transmission electron micrographs of control camel group (Fig. 2d) displayed normal distal tubules with large, rounded nuclei and well-defined nuclear membrane and evenly distributed chromatin material. There were abundant mitochondria with normal cristae, abundant well-defined rough endoplasmic reticulum, free ribosome, some lysosomal bodies, Golgi complex and few cytoplasmic vesicles. There were well-defined and thick basement membranes, intact apical surfaces protruding into lumen, interdigitating membranes extending from the basal lamina towards the apical surface, and normal architecture of synaptic and of gap junctions.

In the dehydrated group (Fig. 2e), the micrographs revealed some normal distal tubular cells whilst others were abnormally small and degenerated with abundant vacuolation and degenerated organelles. Some cells revealed shrunken/pyknotic, indented and/or

degenerated nuclei with condensed chromatin material near the nuclear membrane. Some of the nuclei were without nuclear membrane, were spaced or broken, others showed fragmentation of nuclear material. The mitochondria were swollen, vacuolated, broken or degenerated and ruptured, the ER was sparse and sometimes degenerated. Lysosomes were few with some showing vacuoles whilst others were observed in the tubular lumen. The basement membrane was irregular with uneven thickness, being thin in some areas, full of collagen fibers and on some occasions detached from the cells. The apical plasma membrane seemed to be ruptured in some cells and cytoplasmic material pushed into the tubular lumen with the cellular debris. The lateral plasma membrane was ruptured in some cells, with interdigitating membrane between two cell compartments were sometimes damaged or absent and no synaptic complexes seen. Some connective tissue cells were dead.

In the rehydrated group (Fig. 2f), the micrographs of distal tubular cells in most cases illustrated normal nuclei but a few were pyknotic. The mitochondria, ER and lysosomes appeared normal in structure; however, in few cases they looked degenerated, shrunken, or vacuolated. The cellular basement membranes exhibited a mostly normal appearance but sometimes were partially damaged. The apical plasma membranes were normal in most cases but on few occasions, they were broken and protruded into the lumen with the cytoplasmic debris. Lateral plasma membranes were normal along with well-defined synaptic complexes.

Collecting ducts: transmission electron micrograph

The micrograph of collecting ducts of control camels (Fig. 2g) depicted large nuclei with evenly distributed chromatin material, normal mitochondria, rough endoplasmic reticulum (RER) and a few lysosomes. The basement membrane, dome shaped apical plasma membrane, interdigitating membranes, synaptic complexes were all intact and normal.

The micrograph of collecting ducts of the dehydrated animals (Fig. 2h) showed almost normal cells with large nuclei and intact nuclear membrane with evenly distributed chromatin material, average number of mitochondria, abundant lysosomes, RER, and free ribosomes. The basement membrane looked intact with some collagen materials between it and the connective tissue. Interdigitating membranes were normal with intact gap junctions and the apical plasma membrane were dome shaped and intact. Very few cells showed shrunken/pyknotic nuclei or damaged cytoplasmic organelles.

Micrograph of collecting ducts from rehydrated camels (Fig. 2i) displayed normal cells with large nuclei

and evenly distributed chromatin material. RER, free ribosomes, lysosomes, mitochondria were normal. The basement, luminal and interdigitating membranes were normal and intact, however, in some places the basement membrane was slightly thin. In rare occasions, few nuclei were slightly shrunken, mitochondria not abundant and a few cells were vacuolated.

Measurement of kidney function tests and glucose levels in serum of experimental camels

Serum BUN, Cr, Na⁺, K⁺, Cl⁻, glucose, osmolality and AVP of control, dehydrated and rehydrated camels are presented in Table 3. Dehydration caused a very high increase in serum BUN compared to control ($p < 0.001$), which peaked 2 h after rehydration and started to drop matching control values 12 h post rehydration. BUN levels were statistically lower in rehydrated camels compared to dehydrated groups at 48 and 72 h post rehydration. Cr was significantly higher in dehydrated ($p < 0.001$) and rehydrated ($p < 0.001$) camels compared to controls. However, Cr was lower in rehydrated ($p < 0.001$) camels 72 h later compared to dehydrated group. The concentrations of Na⁺ and Cl⁻ followed a similar pattern and were significantly higher at 20 days of dehydration ($p < 0.01$) and 2 h post rehydration ($p < 0.01$). Na and Cl dropped significantly by rehydration ($p < 0.05$) compared to the dehydrated group but were not significantly different from controls.

Serum K⁺ concentration was not significantly different between the treatment groups till the end of the dehydration period. However, K⁺ values started to rise significantly at 12 ($p < 0.05$), 24 ($p < 0.01$) and 48 h ($p < 0.05$) post rehydration compared to controls. Dehydration caused a significant drop ($p < 0.05$) in glucose concentration. Glucose levels increased significantly ($p < 0.05$) 2 h post rehydration compared to the dehydrated and control values. Between 12–24 h, glucose values fluctuated but were significantly higher ($p < 0.05$) between 48–72 h after rehydration compared to dehydrated values. Dehydration caused a significant rise in calculated osmolality, but values return to normal 12 h onwards post rehydration. AVP was increased significantly by dehydration and remained significantly higher than the control throughout the rehydration period.

Measurement of acute injury markers in kidney cortex and medulla homogenates

Level of MPO, KIM1, NGAL and CRP in kidney cortex and medulla in addition CRP in plasma were measured (Table 4). No significant differences were observed between all three groups of camels.

Table 4 kidney cells biomarkers in renal cortex and medulla of control, dehydrated and rehydrated camels (M±SEM)

Parameter	Tissue type /Plasma	Control	Dehydrated	Rehydrated
MPO ng/mg tissue	Cortex Medulla	21.29±0.8 16.8±0.5	21.0±1.4 17.5±0.5	19.8±1.3 18.1±0.6
KIM1 pg/mg tissue	Medulla Cortex	612.5±32.9 490.3±35.1	592.4±9.9 572.9±22.6	585.0±10.9 573.8±12.1
NGAL ng/mg tissue	Cortex Medulla	29.9±3.2 28.0±1.19	28.8±1.5 27.3±1.2	31.2±2.4 23.7±2.4
CRP µg/mg tissue	Cortex Medulla	0.59±0.04 0.49±0.01	0.61±0.03 0.52±0.03	0.56±0.25 0.49±0.02
CRP (ng/ml)	Plasma	1.4±0.01	1.4±0.01	1.7±0.18

Measurement of fructose and SGLT2 (GLUT2) in kidney cortex and medulla homogenates

Fructose level was generally higher in cortex than medulla. Dehydration caused a significant elevation in fructose levels in both cortex ($p < 0.01$) and medulla ($p < 0.05$) but values significantly decreased ($p < 0.05$) by rehydration to attain control values (Fig. 3a). SGLT2 (GLUT2) depicted no significant change between control and dehydrated camels in both cortex and medulla. SGLT2 (GLUT2) levels were significantly elevated by rehydration in both cortex and medulla ($p < 0.001$) compared to controls (Fig. 3b).

Measurement of uric acid in plasma

Mean uric acid concentration was very low in plasma of control camels. Plasma uric acid content significantly increased by dehydration ($p < 0.01$) and rehydration ($p < 0.01$) but was still low compared to controls (Fig. 4).

However, these results are extremely low compared to human subjects.

Expression of AVPR2 protein and mRNA in kidney cortex and medulla

AVPR2 receptor protein levels were significantly down regulated by dehydration in the cortex and displayed further reduction 72 h after rehydration. However, in the medulla no significant changes were evidenced by dehydration and rehydration (Fig. 5a). At the levels of gene expression, a similar reduction in AVPR2 mRNA levels was seen in the dehydrated cortex compared to controls (Fig. 5b), and levels remained low during rehydration. No transcript changes were seen in the medulla.

Expression of aquaporin proteins and mRNAs in kidney cortex and medulla

Quantification of AQPs 1, 2, 3, 4, 7 and 9 in kidney cortex and medulla of control, dehydrated and

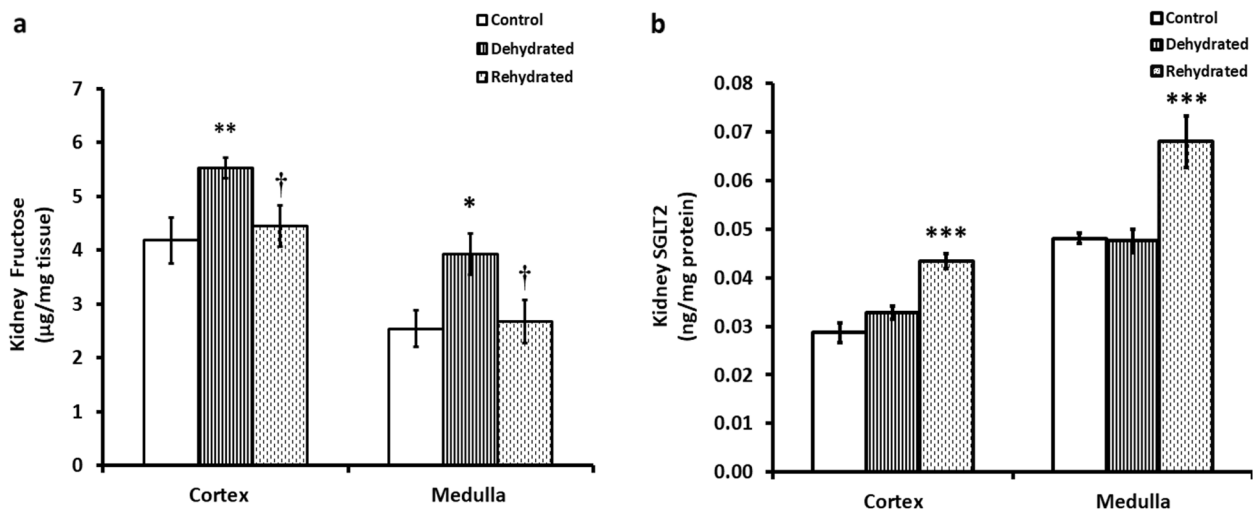


Fig. 3 a Fructose & b SGLT2 levels in kidney cortex and medulla of control, dehydrated and rehydrated camels. Significant difference from Control group denoted by * $p < 0.05$, ** $p < 0.01$, and from Dehydrated (Day 20) group by † $p < 0.05$

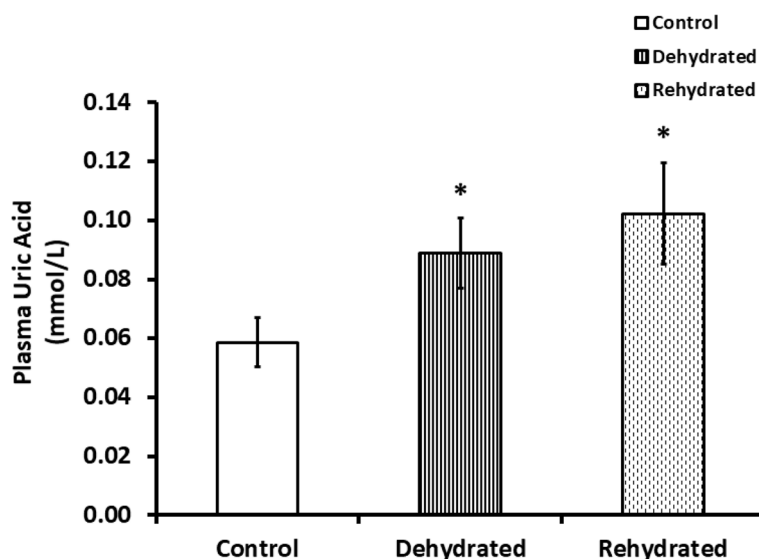


Fig. 4 Uric acid level in plasma of control, dehydrated and rehydrated camels. Significant difference from Control group denoted by * $p < 0.05$

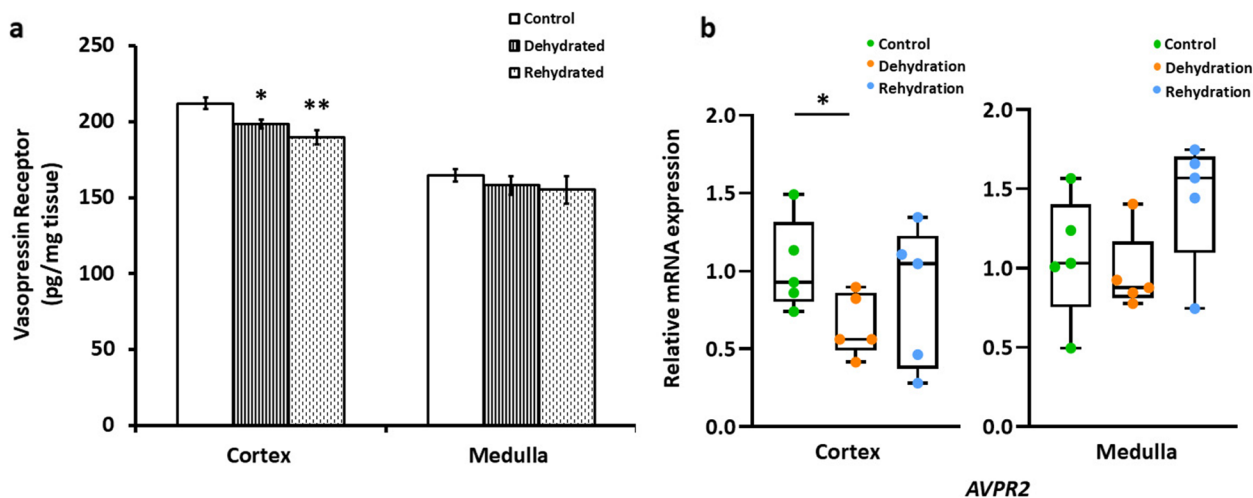


Fig. 5 a AVPR2 (pg/mg kidney tissue) in kidney cortex and medulla of control, dehydrated and rehydrated camels (mean \pm SEM). Significant difference from Control group denoted by * $p < 0.05$, ** $p < 0.01$. **b** Relative mRNA expression of AVPR2, ($n = 5$) in kidney cortex of control, dehydrated and rehydrated camels using qPCR (mean \pm SEM, two-way, unpaired t-test with Welch correction). Significant difference between two groups is denoted by $p < 0.05$; * $p < 0.01$; ** $p < 0.001$; ***

rehydrated camel is presented in Fig. 6a, b, c, d, e, and f respectively. At the protein level, AQP4 was the most abundant in the camel kidney and was slightly more expressed in medulla followed by AQP2 which was also more expressed in medulla followed by AQP3 which was equally expressed in the two compartments and then AQP1 which was also equally expressed in cortex and medulla. AQP7 and AQP9 were very low, and the former was equally expressed in cortex and medulla while the latter was more expressed in cortex.

AQP1 (Fig. 6a) protein increased significantly by dehydration and rehydration in both kidney compartments. The increase of AQP1 protein in cortex after rehydration was significantly higher than dehydration. Transcripts increased in abundance on the cortex following dehydration, but not the medulla [41].

Dehydration caused no change in AQP2 protein levels in cortex but produced a significant decrease in medulla compared to controls. However, control values of AQP2 were restored by rehydration in medulla and over

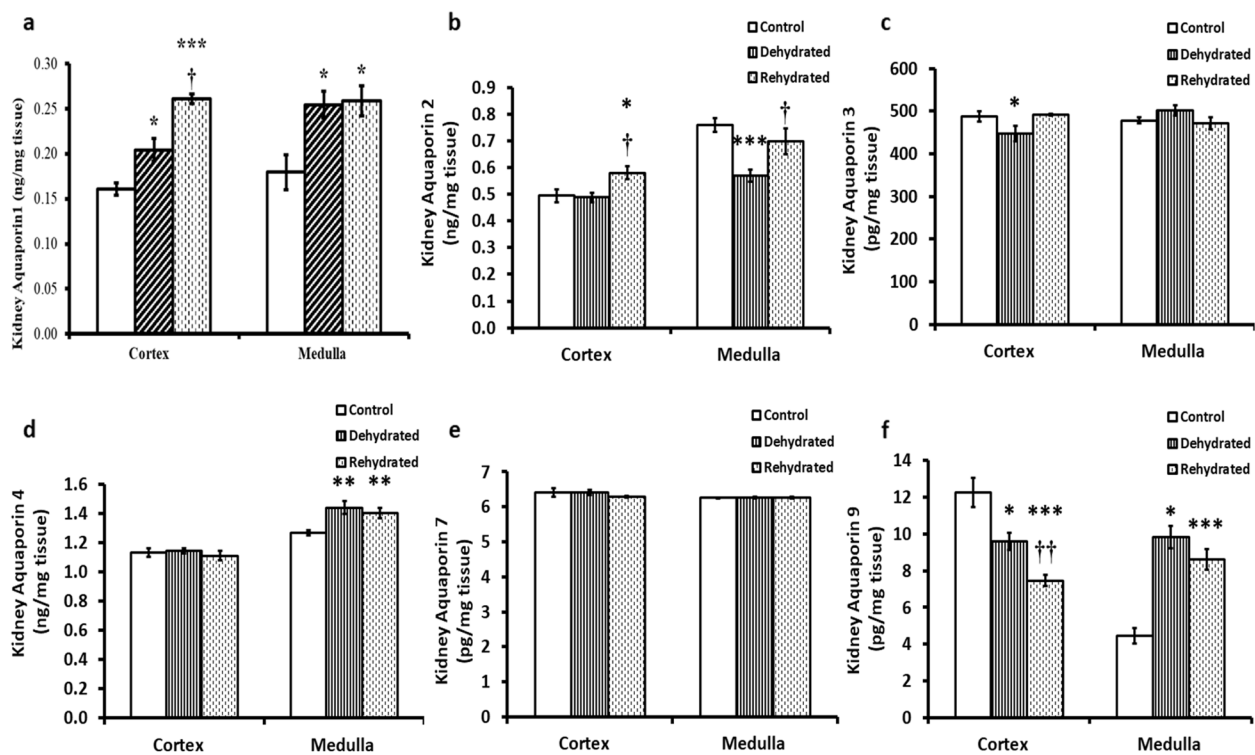


Fig. 6 **a** Aquaporin 1 (ng/mg kidney) in kidney cortex and medulla of control, dehydrated and rehydrated camels ($M \pm SEM$). Significant difference from Control group denoted by * $p < 0.05$, ** $p < 0.01$, *** $p < 0.001$ and from Dehydrated (Day 20) group by † $p < 0.05$, †† $p < 0.01$, ††† $p < 0.001$. **b** Aquaporin 2 (ng/mg kidney) in kidney cortex and medulla of control, dehydrated and rehydrated camels ($M \pm SEM$). Significant difference from Control group denoted by * $p < 0.05$, ** $p < 0.01$, *** $p < 0.001$ and from Dehydrated (Day 20) group by † $p < 0.05$, †† $p < 0.01$, ††† $p < 0.001$. **c** Aquaporin 3 (ng/mg kidney) in kidney cortex and medulla of control, dehydrated and rehydrated camels. (mean + SEM). Significant differences from control is denoted by * $p < 0.05$. **d** Aquaporin 4 (ng/mg kidney) in kidney cortex and medulla of control, dehydrated and rehydrated camels ($M \pm SEM$). Significant difference from Control group denoted by ** $p < 0.01$. **e** Aquaporin 7 (pg/mg kidney) in kidney cortex and medulla of control, dehydrated and rehydrated camels ($M \pm SEM$). No Significant difference between, Control, dehydration, and rehydration groups. **f** Aquaporin 9 (pg/mg kidney) in kidney cortex and medulla of control, dehydrated and rehydrated camels ($M \pm SEM$). Significant difference from Control group denoted by * $p < 0.05$, ** $p < 0.01$, *** $p < 0.001$ and from Dehydrated (Day 20) group by † $p < 0.05$, †† $p < 0.01$, ††† $p < 0.001$

expressed in cortex ($p < 0.05$) (Fig. 6b). At the transcript level, *AQP2* gene expression is increased by dehydration in both cortex and medulla, and returns to control levels following dehydration [41]

AQP3 expression significantly dropped by dehydration in the cortex but levels were restored by rehydration, however in the medulla *AQP3* showed a non-significant increase by dehydration which return to control values by rehydration (Fig. 6c). At the transcript level, *AQP3* gene expression is increased by dehydration in both cortex and medulla and returns to control levels following rehydration [41].

Dehydration exerted no effect on the level of *AQP4* protein in cortex. In the medulla, *AQP4* protein levels were increased by dehydration and rehydration (Fig. 6d).

AQP7 showed a very weak expression in both kidney compartments and its levels were not affected by dehydration or rehydration (Fig. 6e). *AQP9* depicted a weak expression especially in medulla. *AQP9* was

downregulated in cortex by dehydration with a further drop by rehydration. In medulla the levels of *AQP9* significantly increased by dehydration and rehydration (Fig. 6f).

Expression of transcripts encoding *AQPs* 5, 6, 7 and 11 showed non-significant fluctuations in both cortex and medulla by dehydration and rehydration, except for *AQP6*, the expression of which dropped significantly following rehydration in medulla (Fig. 7).

Expression of *SLC9A9* and *SLC26A4* protein and mRNAs in kidney cortex and medulla

Quantification of *SLC9A9* activity values in kidney cortex and medulla are presented in Fig. 8. *SLC9A9* was more active in cortex compared to medulla. *SLC9A9* activity was down regulated ($p < 0.01$) by dehydration in the kidney cortex with a further significant ($p < 0.001$) drop with rehydration compared to control values. In the medulla, *SLC9A9* activity

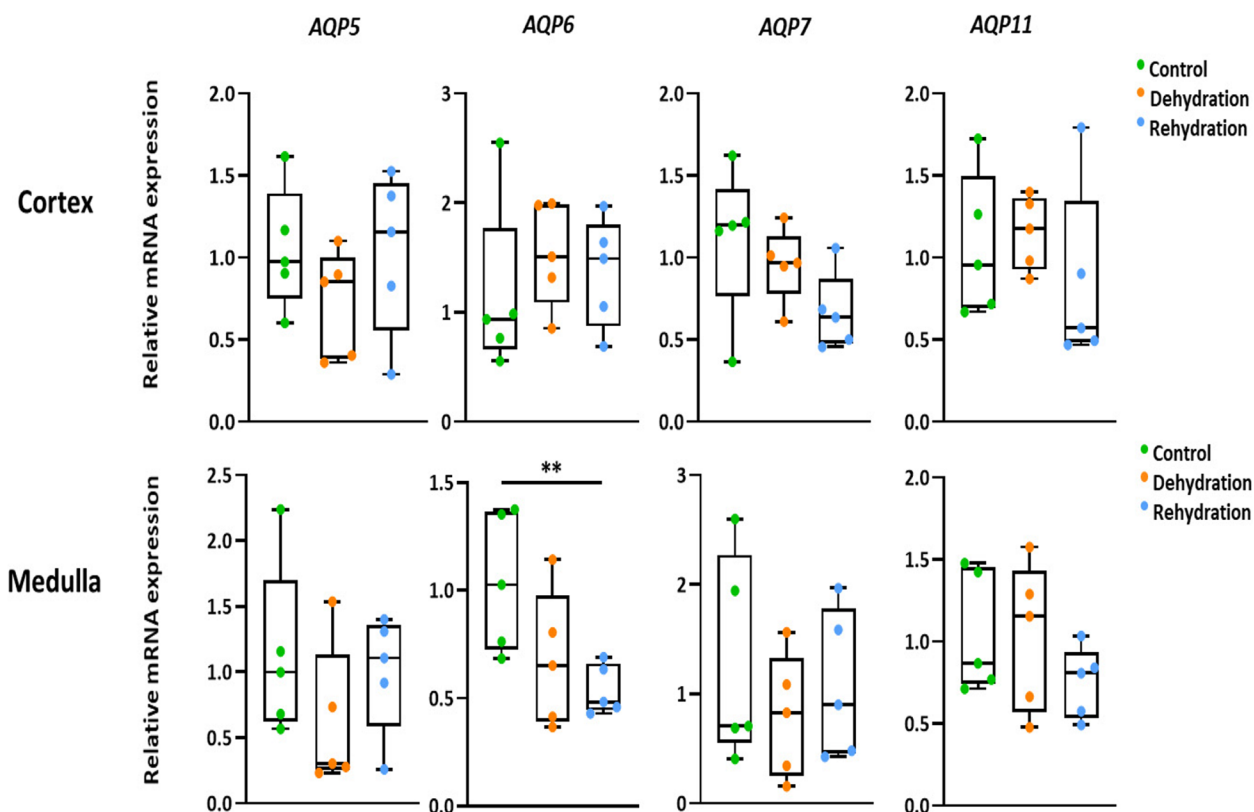


Fig. 7 RT-qPCR validation of genes coding for aquaporins. Relative changes in gene expression in the Arabian camel kidney, medulla and cortex after severe dehydration and acute rehydration compared to controls. Comparison of the means by one-way ANOVA (Turkey's post hoc correction). The boxplots are presented with the S.E.M. ($n=5$), centre lines show median, box edges delineate 25th and 75th percentiles and bars extend to minimum and maximum values. Individual data points represent biologically independent samples and data points within red triangles denote outliers, all the outliers highlighted were included for the statistical analyses. $***p < 0.001$, $**p < 0.01$, $*p < 0.05$

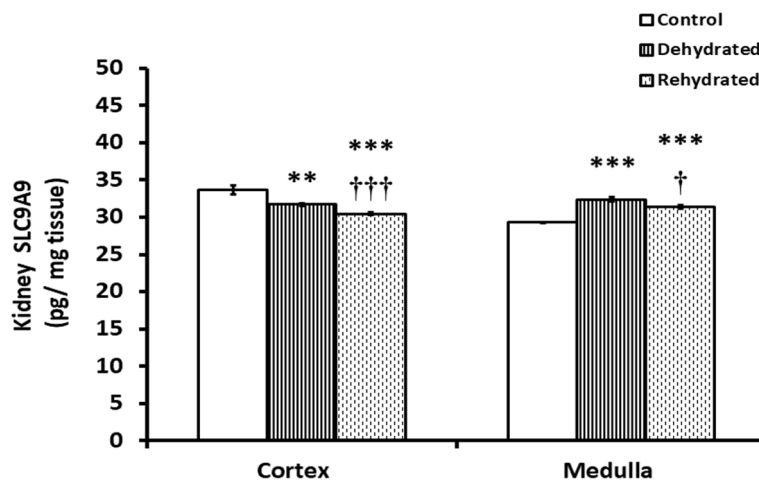


Fig. 8 SLC9A9 (pg/mg kidney) in kidney cortex and medulla of control, dehydrated and rehydrated camels ($M \pm SEM$). Significant difference from Control group denoted by $*p < 0.05$, $**p < 0.01$, $***p < 0.001$ and from Dehydrated (Day 20) group by $^\dagger p < 0.05$, $^\ddagger p < 0.01$, $^\ddagger\ddagger p < 0.001$

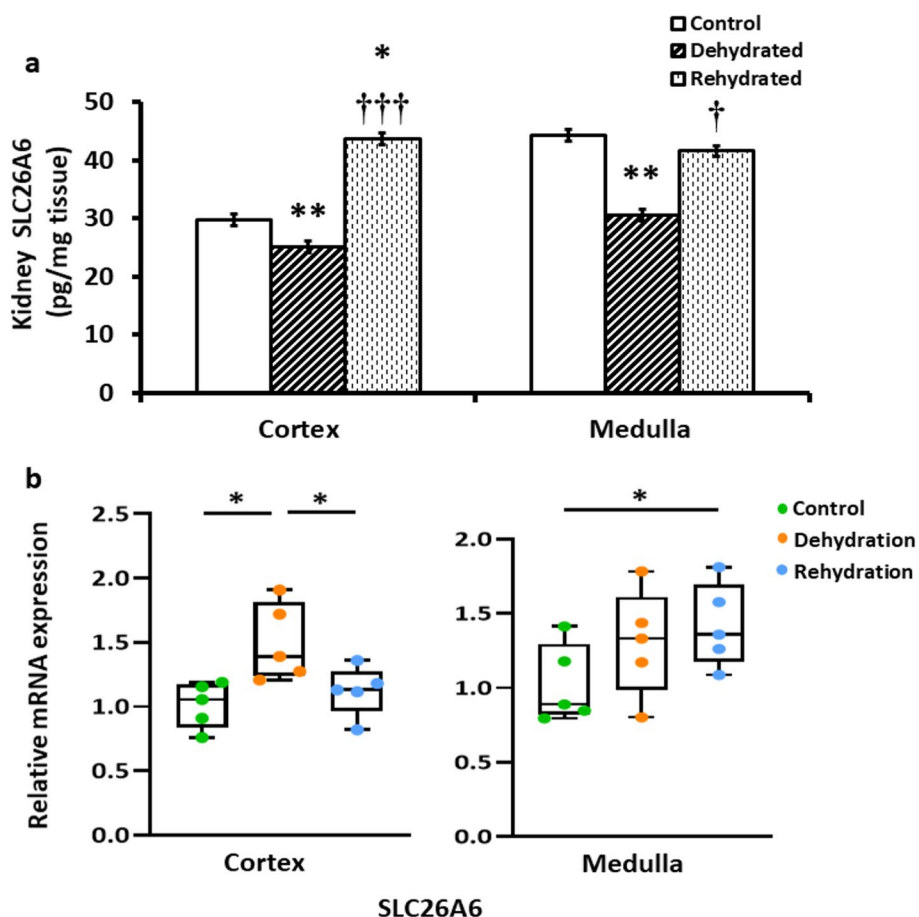


Fig. 9 **a** SLC26A6 (pg/mg kidney) in kidney cortex and medulla of control, dehydrated and rehydrated camels ($M \pm SEM$). Significant difference from Control group denoted by * $p < 0.05$, ** $p < 0.01$, *** $p < 0.001$ and from Dehydrated (Day 20) group by † $p < 0.05$, †† $p < 0.01$, ††† $p < 0.001$. **b** Relative changes in mRNA expression of SLC26A6 ($n = 5$) gene in kidney cortex and medulla of control, dehydrated and rehydrated camels (mean \pm SEM, two-way, unpaired t-test with Welch correction) examined by qPCR. Significant difference between two groups is denoted by $p < 0.05$; * $p < 0.01$; **

increased significantly ($p < 0.001$) by dehydration with slight down regulation with rehydration to a level that was still significantly higher compared to controls ($p < 0.001$). No changes in *SLC9A9* transcript abundance were evident [41].

The carrier protein for oxalate transport SLC 26A6 was higher in medulla compared to cortex (Fig. 9a). SLC26A6 expression was significantly down regulated in cortex and medulla by dehydration. However, SLC26A6 values were significantly upregulated by rehydration in both cortex and medulla compared to values of the dehydrated group. The levels of *SLC26A6* mRNA were significantly upregulated in the cortex by dehydration and dropped significantly by rehydration. In the medulla, the *SLC26A6* mRNA was upregulated especially during rehydration (Fig. 9b).

Measurement of growth factor β (TGF- β) kidney cortex and medulla homogenates

Transforming growth factor β (TGF- β) in the kidney cortex and medulla of control, dehydrated and rehydrated camel is displayed in Fig. 10. There was no significant difference in TGF β values between control, dehydrated and rehydrated camels in cortex and medulla.

Further gene expression measurements in kidney cortex and medulla

The steady-state expression levels of mRNAs encoding proteins involved in different cell activities in the kidney cortex and medulla are presented in Fig. 11.

SLC6A6 mRNA expression displayed a significant increase in both cortex ($P < 0.01$) and medulla ($P < 0.05$) by dehydration and then dropped significantly to control

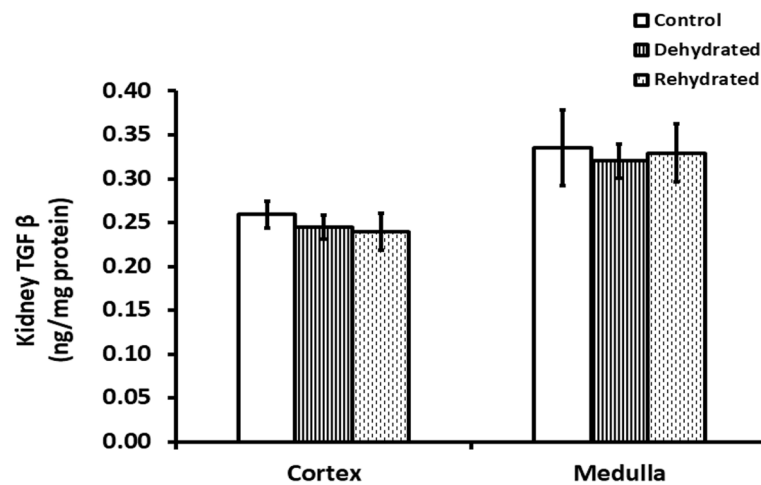


Fig. 10 TGF β (ng/mg kidney tissue) in kidney cortex and medulla of control, dehydrated and rehydrated camels ($M \pm SEM$). No statistical difference was detected

levels in cortex ($P < 0.05$) and medulla ($P < 0.05$). *SLC20a* mRNA expression increased significantly in cortex by dehydration but was unchanged in the medulla. Rehydration induced no effects on *SLC20a* mRNA expression. The expression level of *ATP1A1* mRNA trended downwards in the cortex following dehydration but returned to control values because of rehydration. In the medulla, *ATP1A1* mRNA expression was not changed by dehydration but was significantly increased after rehydration compared to control ($P < 0.05$) and dehydrated ($P < 0.05$) levels. The *PCDH8* mRNA encoding a Ca ion binding protein showed significantly higher ($P < 0.05$) expression level in the cortex following dehydration and rehydration ($P < 0.01$). *PCDH8* expression trended downwards in the medulla following dehydration but returned to control values following rehydration. Expression levels of the *SLC8A1* mRNA, encoding a Na^+/Ca^{++} exchanger protein trended downwards in the cortex, but increased significantly following rehydration ($P < 0.05$) compared to control and dehydrated camels. Expression was unchanged in the medulla.

The steady-state expression level of the *KCNIP4* mRNA, encoding a voltage-gated K channel and Ca binding protein significantly decreased following dehydration in the cortex of dehydrated compared to control ($P < 0.05$) and rehydrated ($P < 0.01$) camels. *KCNIP4* mRNA expression values in medulla exhibited no change by treatment.

Relative mRNA expression of the *SLC2A11* gene, which encodes a protein facilitating glucose cell membrane transport, trended downwards following dehydration in both kidney cortex and medulla but returned to control values because of rehydration. However, there was a significant expression level in cortex ($P < 0.001$) and medulla ($P < 0.001$) of *AMPD2* mRNA encoding enzyme AMP deaminase in purine nucleotide cycle which expedites fructose to form uric acid. The *AMPD2* gene expressed control values by rehydration in both kidney tissues.

NT5dc2 mRNA expression encoding enzyme 5-NT-domain involved in uric acid formation, was upregulated by dehydration in cortex (albeit not significant) and medulla ($p < 0.05$). However, its expression level dropped to attain control values by rehydration in cortex and medulla ($p < 0.01$). The *SLC17A3d* mRNA expression encoding for transporter protein involved in excretion of intracellular urates and organic anion was downregulated in cortex by dehydration albeit not significant. However, the *SLC17A3d* mRNA expression in cortex increased significantly by rehydration ($P < 0.01$). The steady-state *SDHA* mRNA expression level encoding a major subunit protein of succinate dehydrogenase in mitochondria respiratory chain depicted insignificant changes in both cortex and medulla by dehydration and rehydration though the gene expression was slightly increased in cortex and slightly decreased in medulla by dehydration.

(See figure on next page.)

Fig. 11 RT-qPCR validation of the expression of key kidney genes. Relative changes in gene expression of key genes in the Arabian camel kidney cortex and medulla after severe dehydration and acute rehydration compared to controls. Comparison of the means by one-way ANOVA (Turkey's post hoc correction). The boxplots are presented with the S.E.M. ($n = 5$), centre lines show median, box edges delineate 25th and 75th percentiles and bars extend to minimum and maximum values. Individual data points represent biologically independent samples and data points. All the outliers highlighted were included for the statistical analyses. *** $p < 0.001$, ** $p < 0.01$, * $p < 0.05$. Genes are presented in alphanumerical order

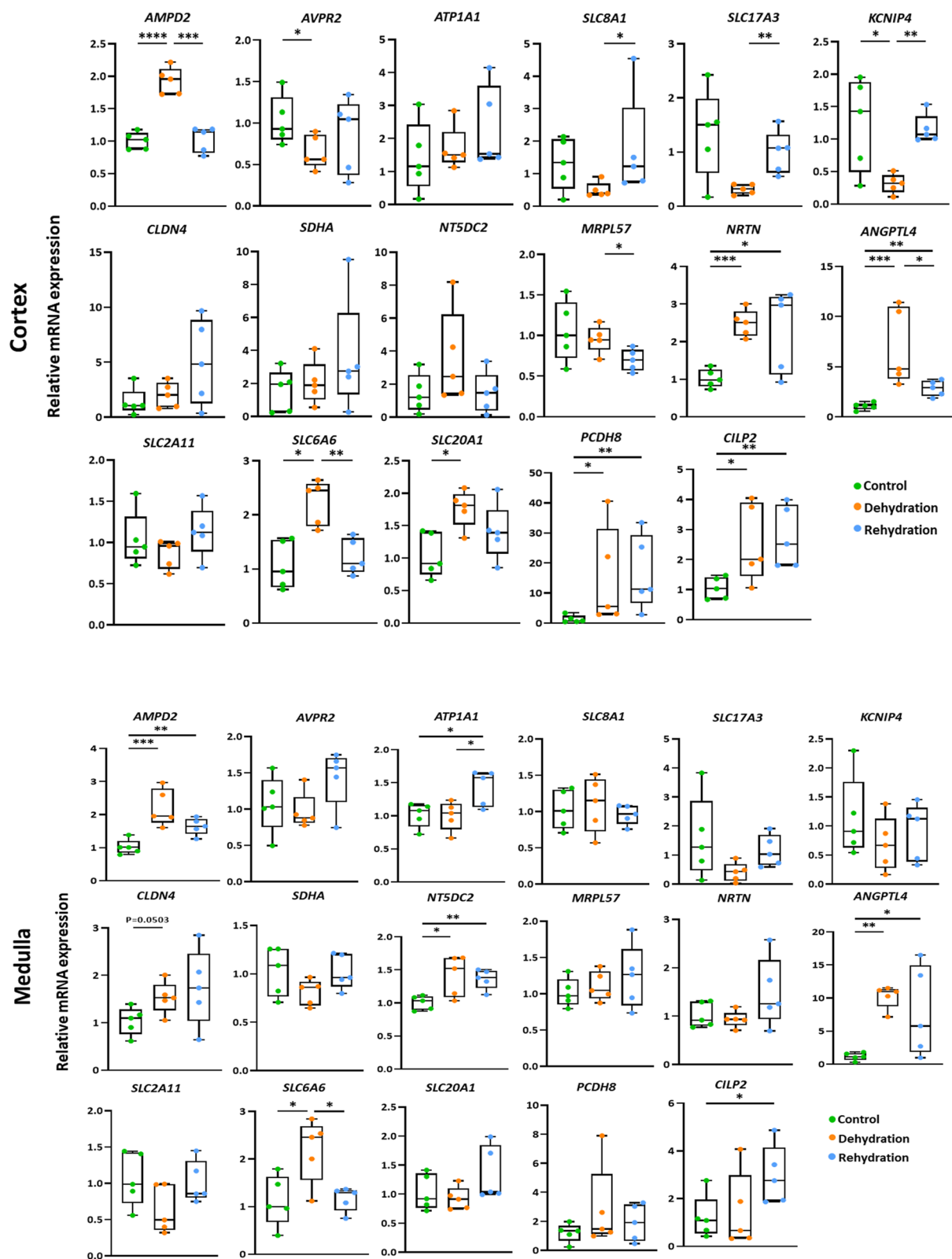


Fig. 11 (See legend on previous page.)

Regarding cytoskeleton of cells there was insignificant upregulation of *CLDN4* mRNA expression level of gene encoding for proteins involved in tight junction of internal organs in cortex and medulla ($P=0.503$) by dehydration. The gene mRNA expression remained high in both cortex and medulla by the short period of rehydration. The expression of steady-state *MRPL57* mRNA that encodes mitochondrial ribosomal protein subunit, depicted a non-significant down regulation in cortex during dehydration but it was significantly down expressed after rehydration ($p<0.05$). The medulla expressed non-significant changes in *MRPL57* mRNA in both periods. The expression level of *NRTN* mRNA coding for Neurturin protein that promotes neuronal survival displayed significant changes during dehydration ($p<0.001$) and rehydration ($p<0.05$) in cortex, but it displayed non-significant changes in the medulla during both periods. *CLIP2* mRNA expression was significantly up regulated in cortex and medulla in both periods. *ANGPTL4* expression normally increases in response to inflammation and hypoxia and acts as apoptosis survival factor for endothelium, modulates vascular permeability and reduces vascular leakage. *ANGPTL4*, mRNA transcript expression level displayed significant increase in cortex compared to control ($p<0.001$) during dehydration but significantly dropped by rehydration ($p<0.05$). However, *ANGPTL4* expression level was significantly increased by dehydration ($p<0.01$) and rehydration ($p<0.05$) in medulla.

Discussion

The camel kidney, with its special morphological characteristics, plays a major role in water conservation during dehydration. In the first part of this communication [30], we reported mild elevation of some pro-inflammatory cytokines, oxidative stress and apoptotic markers mostly in the kidney cortex of the dehydrated and rehydrated camels. In this report, we present, for the first time, mild to moderate histopathological and ultrastructural kidney lesions after long-term dehydration in the camel with a quick rectification of the degenerative changes by rehydration. These lesions included mild vacuolar degeneration and focal necrosis of some epithelium and glomeruli with casts in the tubular lumen. Ultrastructural changes were evident in the kidneys of dehydrated camels, which were mostly observed in some podocytes, mesangial cells, endothelium, and epithelium of proximal and distal convoluted tubules. However, the epithelium of collecting ducts and the interstitial connective tissue in the medulla were mostly refractory or with milder lesions. The cellular changes were generally degenerative in nature including condensation of nuclear chromatin, vacuolization of cytoplasm, swelling of mitochondria, degradation, or loss of brush borders of proximal tubules and degeneration

of lysosomes. However, nuclear pyknosis, karyorrhexes, karyolysis, electron dense apoptotic-like bodies, loss of cellular junctions and synaptic complexes were rarely observed. The slight/moderate EM changes in the kidney cortex of dehydrated camels might have been instigated by the increased levels of pro-inflammatory cytokines (IL-1B, IL-18), apoptosis and oxidative stress biomarkers and accentuated by increased expression of pro-inflammatory (*IL1B* and *IL18* mRNA), apoptotic (*CASP3*, *TP53* mRNA) and MDA (*PTGS1*; *ACSS2*, *GPI* mRNA), levels [30]. Most of these changes were only temporary and largely mitigated but not completely obliterated by short rehydration. It is worth mentioning that pro-inflammatory and oxidative stress biomarkers were not increased in the kidney [30] medulla and that is perhaps why the EM lesions were less marked in that part of the organ.

Certain solute carrier proteins or their mRNA levels might have contributed to the suppression of kidney cellular lesions and/or vital functions, including, *SLC9A9* protein and *ATPIA1*, *CLDN4*, *PCDH8*, *CLIP2*, *NRTN*, *ANGPTL4* and *MRPL57* mRNA expression. Hydrogen ions (H^+) in Golgi apparatus/cellular organelles are exchanged for Na^+ in cytoplasm across their membranes to attain a proton balance and acid base balance by membrane pump where *SLC9A9* act as SLC carrier protein [42]. The significant suppression of *SLC9A9* protein formation and potential retention of H^+ in cellular organelles by dehydration/rehydration might contribute to degenerative changes observed in cortical cell organelles whereas in the medulla the *SLC9A9* had been upregulated with little or no cellular changes. Also, the damage of brush borders observed in EM was accompanied by a tendency of down regulation of the *ATPIA1* mRNA encoding the Na^+/K^+ ATPase of the Na^+/K^+ pump at the brush borders of proximal tubules; perhaps due to effect of hyperosmolality [43]. However, *ATPIA1* mRNA expression was upregulated in cortex by rehydration in concordance with the renewal of brush borders. On the other hand, there was upregulation of several mRNAs encoding proteins that might contribute to the cortical and/or medullar cell stability, integrity, and function to overcome the effects of dehydration. This upregulation included the *CLDN4* mRNA encoding for a component of tight junction protein and *PCDH8* mRNA encoding a calcium-dependent cell-adhesion transmembrane-protein allowing cell-cell contact and cytoskeleton regulation [44]. Similarly, in the cortical region, there was upregulation of the *CLIP2* mRNA encoding a protein mediating interaction between membranous organelles and microtubules, the *NRTN* mRNA encoding the neurturin protein promoting neuronal survival and the *ANGPTL4* mRNA that encodes an apoptosis survival factor protecting endothelium and modulating

vascular permeability. However, there was no change in the expression level of the *SDHA* mRNA encoding succinate dehydrogenase subunit involved in mitochondrial respiration, which indicated a non-disruption of electron transfer chain (ETC) and ATP production. Nonetheless, mitochondrial *MRPL57* mRNA expression level, coding protein subunits of oxidative phosphorylation [45], evidenced a down regulation. This gene and its members act as apoptosis inducing factors when overexpressed [46]. The under expression of *MRPL57* mRNA, normal expression of *SDHA* mRNA and upregulation of *ANGPTL4* mRNA might contribute to ATP production in cortical epithelial cells to prevent at least cleaved PARP1 enzyme from inducing caspase-independent apoptosis during energy crisis [47, 48]. It is worth noting that we reported upregulation in un-cleaved PARP1 but stable *PARP1* mRNA expression during dehydration/rehydration in cortex and medulla [30]. In the medulla, where most cells were normal, the *SLC9A9* protein, *ATPIA1*, *CLDN4*, *PCDH8*, *CLIP2*, *NRTN*, *ANGPTL4* and *MRPL57* mRNAs expressions were either upregulated or within the control values by dehydration/rehydration.

The kidney lesions, mainly in cortex, in dehydrated camels were different from that induced by hypoxia in ischemic renal injury which is characterized by effacement of podocytes and disruption of slit diaphragm [49] and that observed in short dehydration in rabbits, with podocytes and their major processes showing reversible flattening and spreading simulating post-ischemic acute renal failure [24]. Also, the kidney lesions in the dehydrated camel were less marked and totally different from that reported for the Mesoamerican nephropathy/CKD caused by chronic recurrent dehydration in humans. CKD is characterized by interstitial fibrosis, extensive glomerular sclerosis, podocytic injury, atrophy and dilatation of renal tubules, loss of brush borders and acute inflammation resulting from repetitive acute cell injury [26, 50]. These lesions of CKD were accompanied by elevation of serum Cr, increased urine NGAL, reduced GFR, albuminuria, hypernatremia, hypokalemia, and progressive renal failure [22, 51]. We reported increased Cr and BUN and were attributed to insidious kidney lesions observed in histopathology/EM and/or due to loss of body mass but not to acute tubular injury as its biomarkers (NGAL, KIM1), CRP and MPO [52] were not changed in experimental camels.

The net Na retention and other solutes are generally considered to be the hallmark in the hyperosmolar state which drives the consequences of dehydration. In the dehydrated camel, we reported increased serum Na, osmolality, and vasopressin levels. In this context, we also reported upregulation in expression level of the *SLC6A6* mRNA encoding a Na/Cl dependent transporter

protein, the *SLC20a* mRNA encoding a Na⁺/phosphate cotransporter protein and medullary *SLC9A9a* Na/proton exchanger protein, but without change in mRNA *SLC9A9a* expression and down regulation of the *SLC8A1* mRNA which encodes a protein facilitating cellular exit of 4 Na⁺ ions in exchange for one Ca⁺⁺ ion cell entry, hence expediting intracellular Na⁺ retention. The changes in *SLC6A6*; *SLC20a1* and *SLC8A1* mRNA expression levels were rapidly recovered in the cortex by rehydration.

Since long-term dehydration in the camel kidney and CKD in human and animal models share common etiological factors why they do not exhibit similar kidney lesions? It is intriguing to investigate the factors behind these differences. It has been suggested that the lesions induced by intermittent dehydration in CKD are attributed to three factors. These include elevation of vasopressin by hyperosmolality [25], increased endogenous fructose via activation of polyol pathway with ATP depletion [22, 53] and raised uric acid concentration with formation of oxidants species and inflammatory mediators [54]. Vasopressin elevation during dehydration has been implicated in progression of CKD in human and animal models [25]. The long-term dehydration in the camel induced plasma hyperosmolality, vasopressin and cortisol elevation. Nonetheless, AVPR2 receptor was suppressed and *AVPR2* mRNA expression was down regulated in dehydrated camel which could lead to down regulation of AVP-induced signaling, making an obvious difference between the two disease entities. AVPR2 down regulation in our cases could be attributed to desensitization phenomenon induced by long term-exposure to AVP stimulation [55] and/or possibly due to an increased PGE2 which impedes AVPR2 receptor in chronic dehydration by inhibition of its mRNA expression [56]. PGE2 increased following dehydration in different species [57, 58] including camel [59]. However, our RNAseq data [41] revealed no change in *PTGES2* expression following dehydration in the kidney, although significant upregulation is predicted in the medulla following rehydration [41].

It has been hypothesized that activation of the polyol pathway is implicated in CKD through series of enzyme reactions. Thus, during dehydration aldose reductase, rich in the proximal convoluted tubules, is activated by hyperosmolality to reduce glucose to sorbitol where the latter is oxidized to endogenous fructose by sorbitol dehydrogenase [22].

Although fructose levels were significantly elevated in both cortex (30.5 vs control 23.3 nmol/l) and medulla (22 vs control 15 nmol/l) of dehydrated camels compared to controls, the rise constituted only half that reported for kidney cortex of mice model for CKD (60 nmol/l vs 30 control nmol/l) [60] when the results are adjusted

to similar units. These differences may be attributed to sorbitol dehydrogenase activity being generally low in the normal camel [61]. Moreover, there was a significantly lower serum glucose levels during dehydration. Similarly, there was down regulation of *SLC2A11* mRNA expression and normal SGLT2 (GLUT2 protein: facilitates glucose transcellular transport) with limited available glucose for conversion to sorbitol [62]. Therefore, the polyol pathway seems not to be triggered in dehydrated camels to pursue ROS formation to induce kidney injury as in humans. Thus, the fructose handling by this pathway constitutes another difference between humans and camels. The dehydration effects were temporary and *SLC2A11* mRNA expression, tissue fructose and serum glucose assumed control values by rehydration.

Proximal tubular injury in CKD can be induced by the end products of fructose metabolism, such as uric acid, and ATP depletion [25]. Excess endogenous fructose is converted by fructokinase to fructose-1-phosphate resulting in depletion of intracellular ATP and leading to uric acid formation via the involvement of a series of enzymes including AMP deaminase 2 (AMPD2), 5-NT and xanthine oxidase [63]. Intracellular uric acid can induce oxidative stress in vascular smooth muscles, endothelium, kidney tubules etc. via the stimulation of NADPH oxidase or reaction with peroxynitrite to generate oxygen/nitrogen reactive radicles and chemokines [64]. There was a significant relative increase in serum uric acid levels in both dehydrated (0.089 ± 0.02 vs 0.059 ± 0.008 mmol/l) and rehydrated camels (0.102 ± 0.017 mmol/l) along with relative increase in kidney fructose, upregulation of *AMPD2* mRNA and *NT5dc2* mRNA expression levels encoding AMPD and 5-NT enzymes, and downregulation of *SLC17A3d* mRNA expression encoding a voltage-derived transporter protein involved in excretion of intracellular urates. Despite this, the serum uric acid rise was trivial and far below the lowest normal range for humans (0.21–0.42 mmol/l) and mouse (0.12–1.5 mmol/l) [22]. It is worth noting that uric acid concentration is generally low in the camel [65] and the enzyme xanthine oxidase has extremely low levels in camel tissues including the kidneys [61, 66]. Therefore, the uric acid level in dehydrated camels was not high enough to induce kidney lesions as seen in CKD. Tubular interstitial fibrosis/glomerular sclerosis and inflammation are the hallmark of CKD and mediated by TGF- β 1 via stimulation of smad3 or smad7 pathways respectively [67, 68]. When intracellular Ca^{++} rise or influx through activation of Ca^{++} -gated KCa3.1 channel [69], it associates with calmodulin to instigate TGF- β 1 to induce signal transduction to trigger smad pathways [70]. The KCa3.1 channel is encoded by *KCNN4* gene and is controlled by a variety of kinases

and phosphatases [28]. The absence of kidney fibrosis in dehydrated camels as per histopathology and EM results was due to low level activity of this pathway. Our RNAseq data [41] indicates that whilst the *TGFB1* gene is expressed at equivalent levels in both cortex and medulla of the camel kidney, its expression is unchanged by dehydration or rehydration and so is *TGFB1* protein. On the other hand, the *KCCN4* gene is barely expressed at all in the camel kidney; expression levels are very low in both cortex and medulla and are unchanged by dehydration or rehydration. It is worth noting that expression of the *KCNIP4* and *SLC8A* mRNAs encoding proteins related to Ca^{++} regulation/transport [71] were also depressed in the cortex by dehydration. Down regulation of cellular Ca^{++} might be an adaptive mechanism that safeguards cellular organelles during dehydration [72, 73]. *KCNIP4* mRNA and *SLC8A1* mRNA down regulation in cortex was abolished by rehydration, whereas expression in medulla remained at control values during the whole treatment periods.

Dehydration is a risk factor for nephrolithiasis by inducing low-volume saturated urine in human subjects with Ca oxalate nephrolithiasis constituting more than 80% of Ca stones [74, 75]. Camels normally feed on high dietary oxalates and blood ascorbic acid level is naturally high. During dehydration it voids very few drops of highly concentrated urine and shows increased inflammatory markers in kidney cortex [30]. Low urine volume with high oxalate and high Ca^{++} can lead to precipitation of Ca oxalate nephrolithiasis which are very injurious [74]. *SLC26A6* carrier protein, which mediates apical membrane oxalate/Cl exchange, is normally upregulated when oxalates are high in the body [76, 77]. Analysis of *SLC26A6* protein displayed a significant down regulation in both cortex and medulla despite the upregulation of *SLC26A6* mRNA expression. This might suggest that increased turnover of the protein is being compensated by increased transcription of the gene. Taken together, the results of histopathology, EM, serum Ca and *SLC26A6* protein expression might prevent the possibility of nephrolithiasis that could possibly contribute to kidney lesions in the dehydrated camels. It has been observed that kidney tissue damage and apoptosis caused by chronic dehydration are less pronounced in desert species than humans and laboratory animal models and that was attributed to the obvious role of AQP water channels [78]. Moreover, our recent finding that suppressed tissue cholesterol biosynthesis may contribute to water retention by the camel kidney during dehydration [41]. AQPs 1, 2, 3 and 4 channels in kidney cortex and medulla seemed to be indispensable for the camel's durability to long-term dehydration and play an essential role in kidney tissue protection from injuries. AQP1,

mainly located at the apical and/or basolateral membranes of proximal tubules, descending loop of Henle and descending vasa recta, facilitates water passage from tubular lumen to cells with subsequent urine concentration [79, 80]. We reported a significant elevation of *AQP1* mRNA expression in cortex of dehydrated camels [41] along with increased level of AQP1 protein and that the effect was even more pronounced by rehydration. AQP2, located at the distal convoluted tubules and collecting ducts, transports water from tubular lumen into the cells via the apical plasma membrane [81]. The process is facilitated by AVP/AVPR2 ligand/receptor binding to induce urine concentration [82]. AQP2 is also expressed in other organs and can be regulated by estrogen [21]. Dehydration robustly upregulated *AQP2* mRNA expression level in both parts [41] and AQP2 protein in cortex but down regulated in medulla. In general, AQP2 protein level may not necessarily reflect the *AQP2* mRNA levels. For example, availability of the mRNA for translation is sometimes subject to micro-RNA (miRNA) mediated molecule sequestration or degradation [83]. Inappetence observed in dehydrated camels and/or the down regulation of AVPR2 receptors might contribute to AQP2 protein depression in the medulla during dehydration [84]. AQPs 3 & 4 facilitate water passage from cells of distal convoluted tubules and collecting ducts to circulation via basolateral transmembrane transmission against the osmotic gradient [85]. However, these two aquaporins are separately located and regulated [84]. It has been reported that *AQP3* mRNA expression and protein level were upregulated by sustained vasopressin stimulation, whereas *AQP4* expression was not affected [86]. *AQP3* mRNA expression level was significantly upregulated in cortex and medulla by dehydration [41], but AQP 3 channel protein was down regulated in cortex, possibly because of *AQP3* mRNA sequestration, to control water passage to the outside so as to protect the very active cortical cells from stress injuries [83]. AQP3 channel protein levels displayed no change by treatments in medulla, whereas cells are normally less active compared to that in cortex, a process which can facilitate normal water exit to support circulation. *AQP4* mRNA expression was very low in kidney in all groups during the experimental period. Although, AQP4 channel protein exhibited no change by treatment in cortex, its real role in water conservation was reflected in medulla where its levels were increased by dehydration and rehydration possibly to support the general circulation. AQP7, an aquaglyceroporin channel, is mainly expressed in brush borders of proximal convoluted tubules [87] and is extremely low in the camel kidney (pg/g tissue) perhaps due to rapid glycerol fermentation in rumen [88]. AQP7 seemed to play little role, as the channel and *AQP7* mRNA expression

level revealed no changes in either kidney cortex or medulla during the experimental periods despite the partial loss of brush borders. Similarly, the expression of the *AQP9* mRNA and the AQP9 aquaglyceroporin channel in the camel kidney was very low. AQP9, protein which normally expedites passive water transport against osmotic gradient, was downregulated by dehydration and rehydration in the cortex, but significantly increased its expression in medulla against the great osmotic gradient created by the countercurrent multiplier mechanism. Although, we have not measured AQP5, AQP6 proteins and AQP11 aquaglyceroporin channels to draw a genuine conclusion, the expression of the *AQP5*, *AQP6* and *AQP11* mRNAs were largely unaffected by treatment, although the expression of the *AQP6* mRNA was significantly depressed in medulla by rehydration. In conclusion, long-term dehydration in camels caused only temporary histopathological, ultrastructural kidney lesions, possibly induced by mild inflammation, apoptosis, and OS along with gene modulation mostly to favor cell survival. AVP, fructose, uric acid, TGF β and urine oxalate nephrolithiasis seemed to play minor role if at all in inducing severe kidney lesions as that seen in CKD. Modulation of SLC proteins, Aquaporins 1, 2, 3, 4, 7, 9 water channels and regulation of mRNA expression levels during dehydration/rehydration are suggested to play a major role in water conservation and cell survival. Thus, the camel kidney has a remarkable capability to withstand continuous long-term dehydration and quick rehydration that surpasses that of humans and animal models subjected to CKD.

Acknowledgements

We are thankful to Dr. Naserdine Hamadi and Mr. Azim Ullah Shamsul Islam for technical help.

Authors' contributions

Abdu Adem (AA) and David Murphy (DM) planned and advised on the conduct of the study and provided general oversight of its conduct. Mahmoud A. Ali (MAAli), Muna Abdu Adem (MAA), Naheed Amir (NA), and Osman Ali (OA) oversaw the day-to-day progress of the study (caring for the animals, collecting, and delivering tissue and blood samples, measuring body weights, and recording of data). Ernest Adeghate (EA), Hassan Abu Damir (HA), Saeed Tariq (ST) and Naheed Amir (NA) conducted histopathology, electron microscopy and laboratory analysis. Michael P. Greenwood (MPG), Panjiao Lin (PL), Fernando Alvira-Iraizoz (FAI), Benjamin Gillard BG, performed gene analysis, oversaw quality control of the different assays, assembled all data & performed data analysis. HA, MAAli, AA, and DM Participated in writing the manuscript. All authors contributed and approved the submitted version.

Funding

This study was supported by a grant from The United Arab Emirates University (UAEU)-Program for Advanced Research (UPAR-31M242). The group of Dvid Murphy is supported by Medical Research Council (MR/N022807/1) and The Leverhulme Trust (RPG-2017-287).

Availability of data and materials

Transcriptomic data analyses, including raw FASTQ files, bulk RNAseq counts, DESeq2 data and project metadata, have been deposited in NCBI's Gene Expression Omnibus and are accessible through GEO Series accession

number GSE173683 (<https://www.ncbi.nlm.nih.gov/geo/query/acc.cgi?acc=GSE173683>). Electron microscopic and ELISA data could be requested directly from the corresponding author Prof. Abdu Adem.

Data availability

No datasets were generated or analysed during the current study.

Declarations

Ethics approval and consent to participate

The study protocol was approved by the Animal Ethics Committee of the United Arab Emirates University with approval ID No: ERA-2016–4327. During the experimental period all applicable international, national and/or institutional guidelines for the care and use of animals were followed. We would like to confirm that, this work adhered to the ARRIVE list of guidelines for reporting animal research.

Competing interests

The authors declare no competing interests.

Author details

¹Department of Pharmacology, College of Medicine & Health Sciences, United Arab Emirates University, Al Ain, United Arab Emirates. ²Department of Anatomy, College of Medicine & Health Sciences, Emirates University, Al-Ain, United Arab Emirates. ³Molecular Neuroendocrinology Research Group, Bristol Medical School, Translational Health Sciences, University of Bristol, Dorothy Hodgkin Building, Bristol BS13NY, UK. ⁴Department of Pharmacology, College of Medicine and Health Sciences, Khalifa University, P.O. Box 127788, Abu Dhabi, UAE.

Received: 26 March 2024 Accepted: 31 July 2024

Published online: 16 August 2024

References

- Alim FZD, Romanova EV, Tay Y-L, Rahman AYBa, Chan K-G, Hong K-W, et al. Seasonal adaptations of the hypothalamoneurohypophyseal system of the dromedary camel. *PLoS ONE*. 2019;14(6):e0216679. <https://doi.org/10.1371/journal.pone.0216679>.
- Bornstein S. The ship of the desert. The dromedary camel (*Camelus dromedarius*), a domesticated species well adapted to the extreme conditions of aridness and heat. *Rangifer Special Edition*. 1990;3:231–6.
- Schmidt-Nielsen K. *Animal Physiology*, 5th edition – Adaptation and Environment. Cambridge, UK: Cambridge University Press. 1997. <https://doi.org/10.1017/9780511801822>.
- Asiimwe R, Ainembabazi JH, Egeru A, et al. The role of camel production on household resilience to droughts in pastoral and agro-pastoral households in Uganda. *Pastoralism*. 2020;10(5). <https://doi.org/10.1186/s13570-020-0160-x>.
- Kagunyua A, Wanjohi J. Camel rearing replacing cattle production among the Borana community in Isiolo County of Northern Kenya, as climate variability bites. *Pastoralism, Research, Policy and Practice*. 2014;4(13):1–5. <https://doi.org/10.1186/s13570-014-0013-6>.
- Abdu A, Mahmoud Al H, Sheela B, Pathan JY, et al. ANP and BNP responses to dehydration in the one-humped camel and effects of blocking renin-angiotensin system. *PLoS One*. 2012;8(3):e57806.
- Omland T, Hagve T-A. Natriuretic peptides: physiologic and analytic considerations. *Heart Failure Clin*. 2009;5:471–87.
- FlyBase. Gene Group: Solute carrier family, FB 2018_06 released December 2018. 2018.
- Taj Khorshid E, Nollert P, Jensen MØ, Miercke LJ, O'Connell J, Stroud RM, Schulten K. Control of the selectivity of the aquaporin water channel family by global orientational tuning. *Science*. 2002;296(5567):525–30. <https://doi.org/10.1126/science.1067778>. (Bibcode:2002Sci.296.525T).
- Hediger MA, Romero MF, Peng JB, Rolfs A, Takanaga H, Bruford EA. The ABCs of solute carriers: physiological, pathological, and therapeutic implications of human membrane transport proteins Introduction. *Pflueger's Arch*. 2004;447(5):465–8. <https://doi.org/10.1007/s00424-003-1192-y>. (Epub 2003 Nov 18 PMID: 14624363).
- Ouajid O, Kamel B. Physiological particularities of Dromedary (*Camelus dromedarius*) and experimental implications. *Scand J Lab Anim Sci*. 2009;36:19–29.
- Verlander JW. Normal Ultrastructure of the Kidney and Lower Urinary Tract. *Toxicol Pathol*. 1998;26:1–17.
- Darmady EM, Offer J, Prince J, Fay S. The proximal convoluted tubule in the renal handling of water. *Proceedings of the International Congress of Nephrology*. 1963. pp. 461–462. New York: Czechoslovak Academy of Sciences and Excerpta Medica Foundation.
- Safer AM, El-Sayed NK, Abo-Salem K, Alshaer R. Ultrastructure of the nephron of the one-humped camel, *Camelus dromedarius*. *J Morphol*. 1988;198:287–301.
- Abdalla MA, Abdalla O. Morphometric observations on the kidney of the camel. *Camelus dromedaries J Anat*. 1979;129(1):45–50.
- Zhang W, Edwards A. Oxygen transport across vasa recta in the renal medulla. *Am J Physiol Heart Circ Physiol*. 2002;283:H1042–1055.
- Manefield and GW and Tinson AH. *Camels*. In: *Compendium Series C No. 22*, University of Sydney Post Graduate Foundation in Veterinary Science. 1996.
- Olivetti G, Anversa P, Rigamonti W, Vitali-Mazza L, Loud AV. Morphometry of the renal corpuscle during normal postnatal growth and postnatal growth and compensatory hypertrophy. *A Light Microscope Study*. 1977.
- Eissa L, Ali HA, Ismail HI. Histological and ultrastructural study on the Juxtaglomerular apparatus in the kidney of the dromedary camel (camelus dromedaries). *Int J Curr Adv Res*. 2017;6:6776–83.
- Safer AM, Katchburian E. Unusual membrane-bound bodies in the basal lamina of the uriniferous tubules of the camel (*Camelus dromedaries*). *Acta Anat*. 1991;140:156–62.
- Doaa Z, Shireen H, Caceci T. Microscopic anatomy and ultrastructure of the *Camelus dromedarius* ureter. *Eur J Anat*. 2013;17(4):202–8.
- Roncal-Jimenez CA, M.A. Lanaspá T, Jensen L.G. Sanchez-Lozada R.J. Johnson. Mechanisms by Which Dehydration May Lead to Chronic Kidney Disease. *Ann Nutr Metab*. 2015; 66(suppl 3):10–13 <https://doi.org/10.1159/000381239>.
- Ozkan I, Ibrahim CH. Dehydration, skeletal muscle damage and inflammation before the competitions among the elite wrestlers. *J Phys Ther Sci*. 2016;28(162–168):2016.
- Racusen LC, Prozialeck DH, Solez K. Glomerular epithelial cell changes after ischemia or dehydration. Possible role of angiotensin II. *Am J Pathol*. 1984;114(1):157–63.
- Boubry N, Fernandes S. Mild dehydration, vasopressin, and the kidney: animal and human studies. *Eur J Clin Nutr*. 2003;57(Suppl 2):S39–46.
- Wijkstrom J, Leiva R, Elinder CG, Leiva S, Trujillo Z, Trujillo L, Söderberg M, Hultenby K, Wernerson A. Clinical and pathological characterization of Mesoamerican nephropathy: a new kidney disease in central America. *Am J Kidney Dis*. 2013;62:908–18.
- Nagy KA, Gruchacz MJ. Seasonal Water and Energy-Metabolism of the Desert-Dwelling Kangaroo Rat (*Dipodomys merriami*). *Physiol Zool*. 1994;67(6):1461–78.
- Takei Y, Bartolo RC, Fujihara H, Ueta Y, Donald JA. Water deprivation induces appetite and alters metabolic strategy in *Notomys alexis*: unique mechanisms for water production in the desert. *Proc Royal Soc B-Biol Sci*. 2012;279(1738):2599–2608. 10.
- Köhler-Rollefson I, Mundy P, Mathias, A. *Field Manual of Camel Diseases*. Virginia, USA: Stylus Publishing; 2001.
- Ali MA, Hassan Abu Damir I, Osman M Ali, Naheed Amir, Saeed Tariq, Michael P. Greenwood, Panjiao Lin, Benjamin Gillard, David Murphy and Abdu Adem. The effect of long-term dehydration and subsequent rehydration on markers of inflammation, oxidative stress and apoptosis in the camel kidney. *BMC Vet Res*. 2020;16:458. <https://doi.org/10.1186/s12917-020-02628-5>.
- Karnovsky MJ. (1965) A formaldehyde-glutaraldehyde fixative of high osmolarity for use in electron microscopy. *J Cell Biol*. 1965;27:137A.
- Morris JK. A formaldehyde glutaraldehyde fixative of high osmolality for use in electron microscopy. *J Cell Biol*. 1965;27:1A–149A.
- Silva M, Carvalho Guerra F, Magalhaes M. The fixative action of uranyl acetate in electron microscopy. *Experientia*. 1968;24(10):1074–1074.
- Sjostrand FS. A method to improve contrast in high resolution electron microscopy of ultrathin tissue sections. *Exp Cell Res*. 1956;10(3):657–64.
- Reynolds ES. The use of Lead Citrate at high pH as an electron-opaque stain in electron microscopy. *J Cell Bio*. 1963;17:208.

36. Livak KJ, Schmittgen TD. Analysis of relative gene expression data using real-time quantitative PCR and the 2(-delta C(T)) method. *Methods*. 2001;25:402–8.
37. Safer A, Abo-Salem K. Ultrastructure of the nephron of the young camel *Camelus dromedarius*. *J Morphol*. 1991;210(2):101–15.
38. Gholami K, Loh SY, Salleh N, Lam SK, Hoe SZ. Selection of suitable endogenous reference genes for qPCR in kidney and hypothalamus of rats under testosterone influence. *PLoS ONE*. 2017;12(6):e0176368. <https://doi.org/10.1371/journal.pone.0176368>.
39. Liu Y, Beyer A, Aebersold R. On the dependency of cellular protein levels on mRNA abundance. *Cell*. 2016;165(3):535–50.
40. Pfaffl MW. Quantification strategies in real-time PCR. The Real-Time PCR Encyclopedia A-Z of quantitative PCR (Bustin SA ed.). Published by International University Line, La Jolla, CA, Chapter 3. 2004. pp. 87–112.
41. Alvira-Iraizoz F, Gillard BT, Lin P, Paterson A, Pauža AG, Ali MA, Alabisi AH, Burger PA, Hamadi N, Adem A, Murphy D, Greenwood MP. Multiomic analysis of the Arabian camel (*Camelus dromedarius*) kidney reveals a role for cholesterol in water conservation. *Commun Biol*. 2021;4(1):779. <https://doi.org/10.1038/s42003-021-02327-3>.
42. Bobulescu IA, Moe OW. Na⁺/H⁺ exchangers in renal regulation of acid-base balance. *Semin Nephrol*. 2006;26(5):334–44. <https://doi.org/10.1016/j.semnephrol.2006.07.001>. (PMCID:2878276;PMID17071327).
43. Takayama M, Nonoguchi H, Yang T, Machida K, Terada Y, Owada A, Tomita K, Marumo F. Acute and chronic effects of hyperosmolality on mRNA and protein expression and the activity of Na-K-ATPase in the IMCD. *Exp Nephrol* Jul-Aug. 1999;7(4):295–305.
44. Duguay D, Foty RA, Steinberg MS. Cadherin-mediated cell adhesion and tissue segregation: qualitative and quantitative determinants. *Dev Biol*. 2003;253(2):309–23. [https://doi.org/10.1016/S0012-1606\(02\)00016-7](https://doi.org/10.1016/S0012-1606(02)00016-7). (PMID12645933).
45. Huang G, Li H, Zhang H. Abnormal Expression of Mitochondrial Ribosomal Proteins and Their Encoding Genes with Cell Apoptosis and Diseases. *Int J Mol Sci*. 2020;21(22):8879. <https://doi.org/10.3390/ijms21228879>. (PMID:33238645;PMCID:PMC7700125).
46. Sun L, Liu Y, Frémont M, Schwarz S, Siegmund M, Matthies R, Jost JP. A novel 52 kDa protein induces apoptosis and concurrently activates c-Jun N-terminal kinase 1 (JNK1) in mouse C3H10T1/2 fibroblasts. *Gene*. 1998;208:157–66.
47. Morales JC, Li L, Fattah FJ, Dong Y, Bey EA, Patel M, Gao J, Boothman DA. Review of Poly (ADP-ribose) Polymerase (PARP) Mechanisms of Action and Rationale for Targeting in Cancer and Other Diseases. *Crit Rev Eukaryot Gene Expr*. 2014;24:15–28.
48. Yang Y, Zhao S, Song J. Caspase-dependent apoptosis and -independent poly (ADP-ribose) polymerase cleavage induced by transforming growth factor beta1. *Int J Biochem Cell Biol*. 2004;36(2):223–34. [https://doi.org/10.1016/S1357-2725\(03\)00215-2](https://doi.org/10.1016/S1357-2725(03)00215-2).
49. Eckardt KU, Bernhardt WM, Weidemann A, Warnecke C, Rosenberger C, Wiesener MS, Willam C. Role of hypoxia in pathogenesis in renal disease. *Kidney Int*. 2005;68:S46–51.
50. Nakayama T, Kosugi T, Gersch M, et al. Dietary fructose causes tubulointerstitial injury in the normal rat kidney. *Am J Physiol Renal Physiol*. 2010;298:F712–20.
51. Hilliard LM, Mirabito Colafella KM, Bulmer LL, Puelles VG, Singh RR, Ow CPC, Gaspari T, Drummond GR, Evans RG, Vinh A, Denton KM. Chronic recurrent dehydration associated with periodic water intake exacerbates hypertension and promotes renal damage in male spontaneously hypertensive rats. *Sci Rep*. 2016;6:33855. <https://doi.org/10.1038/srep33655>.
52. Pepys MB, Hirschfield GM. C-reactive protein: a critical update. *J Clin Invest*. 2003;111:1805–12. <https://doi.org/10.1172/JCI18921>.
53. Diggle CP, Shires M, Leitch D, et al. Ketoheokinase: expression and localization of the principal fructose-metabolizing enzyme. *J Histochem Cytochem*. 2009;57:763–74.
54. Glushakova O, Kosugi T, Roncal C, et al. Fructose induces the inflammatory molecule ICAM-1 in endothelial cells. *J Am Soc Nephrol*. 2008;19:1712–20.
55. Marie1 B, Anaid A, Axel PN T, Stephanie G. Desensitization of the Human V2 Vasopressin Receptor homologous effects in the absence of heterologous desensitization. *J Biol Chem*. 1992;267(1):11783–11788.
56. Machida K, Wakamatsu S, Izumi Y, Yosifovska T, Matsuzaki T, Nakayama Y, Kohda Y, Inoue T, Saito H, Tomita K, Nonoguchi H. Downregulation of the V2 vasopressin receptor in dehydration: mechanisms and role of renal prostaglandin synthesis. *Am J Physiol Renal Physiol*. 2007;292(4):F1274–82. <https://doi.org/10.1152/ajprenal.00154.2006>.
57. Park F, Koike G, Cowley JRAW. Regional time-dependent changes in vasopressin V2 receptor expression in the rat kidney during water restriction. *Am J Physiol Renal Physiol*. 1998;274:F906–13.
58. Zucker A, Nasjletti A, Schneider EG. Effect of water deprivation on urinary excretion of PGE2 in the dog. *Am J Physiol Regul Integr Comp Physiol*. 1983;245:R329–33.
59. Ali MA, Damir HA, Amir N, Adeghate EA, Bastaki S, Murphy D, Adem A. Effects of long-term dehydration on oxidative stress, apoptotic markers and neuropeptides in the gastric mucosa of the dromedary camel. *Mol Cell Biochem*. 2019;455(1–2):109–18. <https://doi.org/10.1007/s11010-018-3474-x>. (Epub 2018 Nov 26).
60. Roncal Jimenez CA, Ishimoto T, Lanaspá MA, Rivard CJ, Nakagawa T, Ejaz AA, Cicerchi C, Inaba S, Le M, Miyazaki M, Glaser J, Correa-Rotter R, González MA, Aragón A, Wesseling C, Sánchez-Lozada LG, Johnson RJ. Fructokinase activity mediates dehydration-induced renal injury. *Kidney Int*. 2014;86(2):294–302. <https://doi.org/10.1038/ki.2013.492>. (Epub 2013 Dec 11).
61. Abu Damir H, Ali MA, Khalafalla AE. Investigation of different enzyme markers in some pathological disorders of the dromedary camels in comparison with other species. *CAP Rev*. 2018;12(041):1–46.
62. Leturque A, Brot-Laroche E, Le Gall M, Stolarczyk E, Tobin V. The role of GLUT2 in dietary sugar handling. *J Physiol Biochem*. 2005;61:529–37.
63. Johnson RJ, Nakagawa T, Sanchez-Lozada LG, Shafiu M, Sundaram S, Le M, Ishimoto T, Sautin YY, Lanaspá MA. Sugar, Uric Acid, and the Etiology of Diabetes and Obesity. *Diabetes*. 2013;62:3307–15.
64. Sánchez-Lozada LG, García-Arroyo FE, Gonzaga G, Silverio O, Blas-Marrón MG, Muñoz-Jimenez I, Tapia E, Osorio-Alonso H, Madero M, Roncal-Jiménez CA, Weiss I, Glaser J, Johnson RJ. Kidney Injury from Recurrent Heat Stress and Rhabdomyolysis: Protective Role of Allopurinol and Sodium Bicarbonate. *Am Nephrol*. 2018;48:339–48. <https://doi.org/10.1159/000494663>.
65. Al-Ali AK, Husayni AH, Power DM. A comprehensive biochemical analysis of the blood of the camel (*Camelus dromedarius*). *Comp Biochem Physiol*. 1988;89B:35–7.
66. Al-Seeni AE. Tissue distribution of Molybdenum hydroxylase, aldehyde oxidase and xanthine oxidase in the male and female camels. *Global J Biochem*. 2009;4:43–6.
67. Gu YY, Liu XS, Huang XR, Yu XQ, Lan HY. Diverse Role of TGF-β in kidney disease. *Front Cell Dev Biol*. 2020;8:123. <https://doi.org/10.3389/fcell.2020.00123>. (Published 2020 Feb 28).
68. Kim SI, Choi ME. TGF-β-activated kinase-1: New insights into the mechanism of TGF-β signaling and kidney disease. *Kidney Res Clin Pract*. 2012;31(2):94–105. <https://doi.org/10.1016/j.krcp.2012.04.322>.
69. Sforna L, Megaro A, Pessia M, Franciolini F, Catacuzzeno L. Structure, Gating and Basic Functions of the Ca²⁺-activated K Channel of Intermediate Conductance. *Curr Neuropharmacol*. 2018;16(5):608–17. <https://doi.org/10.2174/1570159X15666170830122402>.
70. Chunling Huang, Margot L. Day, Philip Poronnik, Carol A. Pollock, Xin-Ming Chen (2013) Inhibition of KCa3.1 suppresses TGF-β1 induced MCP-1 expression in human proximal tubular cells through Smad3, p38 and ERK1/2 signaling pathways; 2013; *Int J Biochem Cell Biol*. 47(1). <https://doi.org/10.1016/j.biocel.2013.11.017>.
71. Morohashi Y, Hatano N, Ohya S, Takikawa R, Watabiki T, Takasugi N, Imaizumi Y, Tomita T, Iwatsubo T. Molecular cloning and characterization of CALP/KCHIP4, a novel EF-hand protein interacting with presenilin 2 and voltage-gated potassium channel subunit Kv4. *J Biol Chem*. 2002;277(17):14965–75. <https://doi.org/10.1074/jbc.M200897200>. (PMID11847232).
72. Cebolla B, Fernandez-Perez A, Perea G, Araque A, Vallejo M. DREAM Mediates cAMP-dependent, Ca²⁺-induced stimulation of GFAP gene expression and regulates cortical astroglialogenesis. *J Neurosci*. 2008;28:6703–13. <https://doi.org/10.1523/JNEUROSCI.0215-08.2008>.
73. Néant I, Haiech J, Kilhoffer MC, Aulestia FJ, Moreau M, Leclerc C. Ca²⁺-Dependent Transcriptional Repressors KCNIP and Regulation of Prognosis Genes in Glioblastoma. *Front Mol Neurosci*. 2018;11:472. <https://doi.org/10.3389/fnmol.2018.00472>. (Published 2018 Dec 18).
74. Han H, Segal AM, Seifter JL, Dwyer JT. Nutritional Management of Kidney Stones (Nephrolithiasis). *Clin Nutr Res*. 2015;4(3):137–52. <https://doi.org/10.7762/cnr.2015.4.3.137>.

75. Yang X, Yao S, An J, Jin H, Wang H, Tuo B. SLC26A6 and NADC-1: Future direction of nephrolithiasis and calculus-related hypertension research (Review). *Mol Med Rep*. 2021;24(5):745. <https://doi.org/10.3892/mmr.2021.12385>. (Epub 2021 Aug 30).
76. Jiang Z, Grichtchenko II, Boron WF, et al. Specificity of anion exchange mediated by mouse SLC26A6. *J Biol Chem*. 2002;277:33963–7.
77. Jiang, et al. High expression of SLC26A6 in the kidney may contribute to renal calcification via an SLC26A6-dependent mechanism. *Peer J*. 2018;6:e5192. <https://doi.org/10.7717/peerj.5192>.
78. MacManes M. Severe acute dehydration in a desert rodent elicits a transcriptional response that effectively prevents kidney injury. *bioRxiv*. 2017. <https://doi.org/10.1101/103077>.
79. Agre P, Preston GM, Smith BL, Jung JS, Raina S, Moon C, Guggino WB, Nielsen S. Aquaporin CHIP: the archetypal molecular water channel. *American Journal of Physiology – Renal Physiology* 265, F463–F476 of kidney disease? *Nat Rev Nephrol*. 1993;2013(9):223–39.
80. Agre P, Sasaki S, Chrispeels J. Aquaporins: a family of water channel proteins. *Am J Physiol Renal Physiology*. 1993;265:F461.
81. Tingskov SJ, Mutsaers HAM, Nørregaard R. Chapter Eleven - Estrogen regulates aquaporin-2 expression in the kidney in Vitamins and Hormones. Volume 112. 2020. pp. 243–264.
82. Garrahy A, Thompson CJ. Vasopressin in: *Encyclopedia of Endocrine Diseases (Second Edition)*. 2019;2:29–35.
83. Alsaleh G, Guttenberg JE. Characterization of microRNAs and their targets. *Methods Mol Biol*. 2014;1142:55–63. https://doi.org/10.1007/978-1-4939-0404-4_7. PMID: 24706275.
84. Arnsfang EC, Sundbye S, Nelson WJ, Nejsum LN. Aquaporin-3 and aquaporin-4 are sorted differently and separately in the trans-Golgi network. *PloS One*. 2013;8(9):e73977. <https://doi.org/10.1371/journal.pone.0073977>. (Published 2013 Sep 18).
85. Toshiyuki Matsuzaki, Tomoyuki Yaguchi, Kinue Shimizu, Aoi Kita, Kenichi Ishibashi & Kuniaki Takata. The distribution and function of aquaporins in the kidney: resolved and unresolved questions. *Anatomical Science International* volume 92. 2017. pp. 187–199.
86. Terris J, Ecelbarger CA, Nielsen S, Knepper MA. Long-term regulation of four renal aquaporins in rats. *Am J Physiol*. 1996;271:F414–22.
87. Sohara E, Rai T, Sasaki S, Uchida S. Physiological roles of AQP7 in the kidney: Lessons from AQP7 knockout mice. *Biochim Biophys Acta*. 2006;1758(8):1106–10. <https://doi.org/10.1016/j.bbame.2006.04.002>. (Epub 2006 Apr 20 PMID: 16860289).
88. Khattab MSA. Glycerol as Feedstuff for Ruminant. *Science International*. 2015;3:90–4. <https://doi.org/10.17311/sciintl.2015.90.94>.

Publisher's Note

Springer Nature remains neutral with regard to jurisdictional claims in published maps and institutional affiliations.